2007-04-26

Sea level variability in the Arctic Ocean from AOMIP models

Proshutinsky, Andrey; Ashik, Igor M.; Hakkinen, Sirpa M. A.; Hunke, Elizabeth C.; Krishfield, Richard A.; Maltrud, Mathew E.; Maslowski, Wieslaw; Zhang, Jinlun

American Geophysical Union

Journal of Geophysical Research 112 (2007): C04S08, doi:10.1029/2006JC003916.
http://hdl.handle.net/10945/62432

JOURNAL OF GEOPHYSICAL RESEARCH, VOL. 112, C04S08, doi:10.1029/2006JC003916, 2007

Sea level variability in the Arctic Ocean from AOMIP models

A. Proshutinsky,[1] I. Ashik,[2] S. Häkkinen,[3] E. Hunke,[4] R. Krishfield,[1] M. Maltrud,[4] W. Maslowski,[5] and J. Zhang[6]

Received 3 September 2006; revised 13 February 2007; accepted 9 March 2007; published 26 April 2007.

[1] Monthly sea levels from five Arctic Ocean Model Intercomparison Project (AOMIP) models are analyzed and validated against observations in the Arctic Ocean. The AOMIP models are able to simulate variability of sea level reasonably well, but several improvements are needed to reduce model errors. It is suggested that the models will improve if their domains have a minimum depth less than 10 m. It is also recommended to take into account forcing associated with atmospheric loading, fast ice, and volume water fluxes representing Bering Strait inflow and river runoff. Several aspects of sea level variability in the Arctic Ocean are investigated based on updated observed sea level time series. The observed rate of sea level rise corrected for the glacial isostatic adjustment at 9 stations in the Kara, Laptev, and East Siberian seas for 1954–2006 is estimated as 0.250 cm/yr. There is a well pronounced decadal variability in the observed sea level time series. The 5-year running mean sea level signal correlates well with the annual Arctic Oscillation (AO) index and the sea level atmospheric pressure (SLP) at coastal stations and the North Pole. For 1954–2000 all model results reflect this correlation very well, indicating that the long-term model forcing and model reaction to the forcing are correct. Consistent with the influences of AO-driven processes, the sea level in the Arctic Ocean dropped significantly after 1990 and increased after the circulation regime changed from cyclonic to anticyclonic in 1997. In contrast, from 2000 to 2006 the sea level rose despite the stabilization of the AO index at its lowest values after 2000.

Citation: Proshutinsky, A., I. Ashik, S. Häkkinen, E. Hunke, R. Krishfield, M. Maltrud, W. Maslowski, and J. Zhang (2007), Sea level variability in the Arctic Ocean from AOMIP models, *J. Geophys. Res.*, *112*, C04S08, doi:10.1029/2006JC003916.

1. Introduction

[2] The ability of models to represent seasonal and interannual variability of sea surface height (SSH) is an important indicator of model validity because sea level (SL) or SSH reflects changes in practically all dynamic and thermodynamic processes of terrestrial, oceanic, atmospheric, and cryospheric origin. Approximately 70 tide-gauge stations in the Barents and Siberian Seas (Kara, Laptev, East Siberian, and Chukchi Seas) have recorded SL changes from the 1950s through the 2000s (Table 1 and Figure 1 in *Proshutinsky et al.* [2004]). These data are available for model validation at the Permanent Service for Mean Sea Level archive (http://www.pol.ac.uk/psmsl/pub/nucat.dat) and at the Woods Hole Oceanographic Institution web site (http://www.whoi.edu/science/PO/arcticsealevel).

[3] Figure 1 shows the longest SL time series from 9 coastal stations in the Siberian Seas (see Figure 2 and Table 1 for station locations). There is a positive SL trend along the Arctic coastlines. For 1954–1989 the rate of SL rise for these stations was estimated as 0.194 cm/yr [*Proshutinsky et al.*, 2004]. Adding 1990–2006 data increases the estimated rate for these stations to 0.25 cm/yr. The SL time series correlates relatively well with the annual AO index (source: NOAA National Weather Service Climate Prediction Center http://www.cpc.noaa.gov), SLP at the North Pole (source: NCAR/NCEP reanalysis product) and SLP at the coastal stations mentioned above. Consistent with the influences of AO-driven processes, the SL dropped significantly after 1990 and increased after the circulation regime changed from cyclonic to anticyclonic in 1997 (*Proshutinsky and Johnson* [1997], updated).

[4] In contrast, from 2000 to 2006 the SL increased in spite of steady low AO index. Because of the large interannual variability, it is difficult to evaluate the significance of this change, but an analysis of model results can provide some insight into these recently observed changes. Of course, this is only possible if the model results agree well with the observational data. The major purpose of this study is to validate AOMIP models against SL observations by determining their major differences and causes for those differences. A second goal of this paper is to recommend

[1]Department of Physical Oceanography, Woods Hole Oceanographic Institution, Woods Hole, Massachusetts, USA.
[2]Arctic and Antarctic Research Institute, St. Petersburg, Russia.
[3]Goddard Space Flight Center, Greenbelt, Maryland, USA.
[4]Los Alamos National Laboratory, Los Alamos, New Mexico, USA.
[5]Department of Oceanography, Naval Postgraduate School, Monterey, California, USA.
[6]Polar Science Center, University of Washington, Seattle, Washington, USA.

0148-0227/07/2006JC003916$09.00

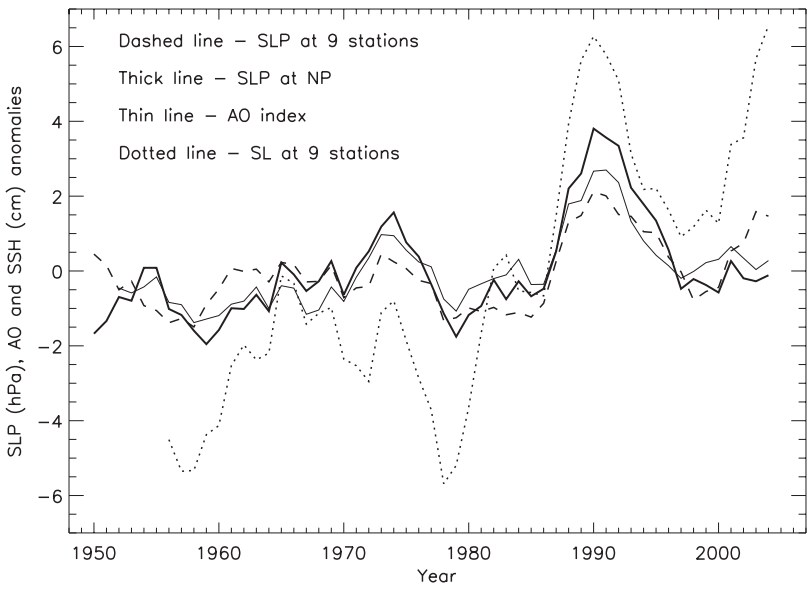

Figure 1. Correlations among SSH, annual AO index and SLP or inverted barometer effect (IBE). Dotted line depicts 5-year running mean SL anomalies averaged for 9 stations representing Siberian Seas. The annual AO index anomalies multiplied by 3 are shown by thin line. The anomalies of the atmospheric pressure averaged for 9 stations (dashed line) and at the North Pole (thick line) both multiplied by −1 represent the IBE.

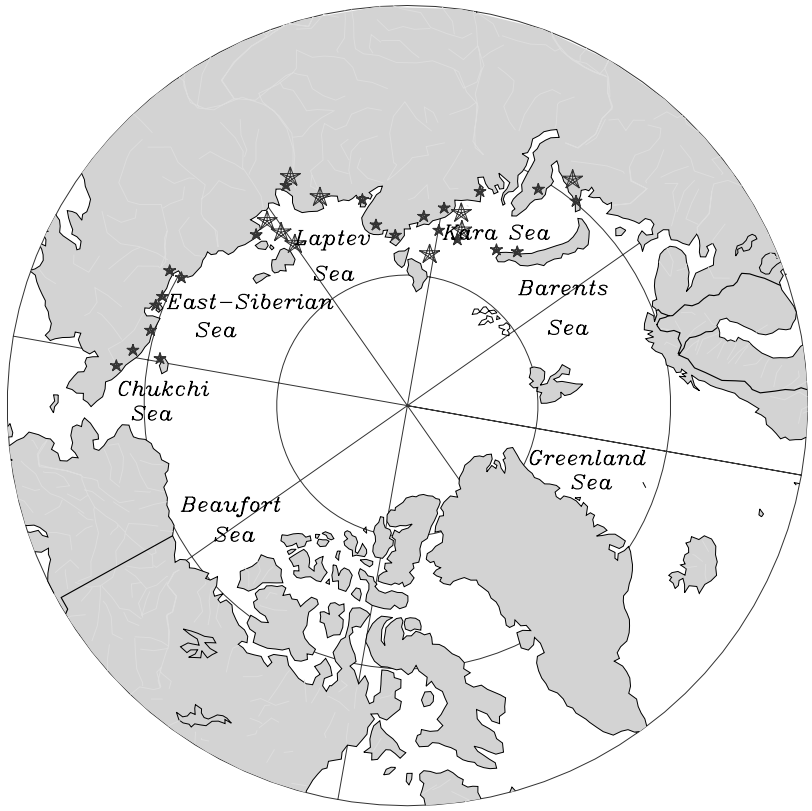

Figure 2. Tide gauge locations are shown as stars (see Table 1 for site names and coordinates). Large stars indicate locations of the 9 stations with the longest records.

Table 1. Stations With SL Data (See Also Figure 1)

Station Number and Name	Latitude	Longitude	Period, years	Station Number and Name	Latitude	Longitude	Period, years
1 Bolvanskii Nos	70.450N	59.083 E	1951–92	2 Amderma[a]	69.750 N	61.700 E	1950–06
3 Russkaia Gavan'	76.183 N	62.583 E	1953–92	4 Harasavei	71.417 N	67.583 E	1954–93
5 Zhelania	76.950 N	68.550 E	1951–95	6 Dikson	73.500 N	80.400 E	1950–96
7 Uedinenia	77.500 N	82.200 E	1953–94	8 Izvestii CIK[a]	75.950 N	82.950 E	1954–06
9 Sterlegova	75.417 N	88.900 E	1950–94	10 Isachenko	77.150 N	89.200 E	1954–92
11 Golomianyi[a]	79.550 N	90.617 E	1954–06	12 Pravdy	76.267 N	94.767 E	1950–93
13 Fedorova	77.717 N	104.300 E	1950–99	14 Andreia	76.750 N	110.750 E	1951–98
15 Preobrazhenia	74.667 N	112.933 E	1951–90	16 Dunai[a]	73.933 N	124.500 E	1951–06
17 Tiksi[a]	71.583 N	128.917 E	1949–06	18 Muostakh	71.550 N	130.033 E	1951–94
19 Kotel'nyi[a]	76.000 N	137.867 E	1951–06	20 Sannikova[a]	74.667 N	138.900 E	1950–06
21 Kigiliakh	73.333 N	139.867 E	1951–99	22 Shalaurova[a]	73.183 N	143.233 E	1950–06
23 Ambarchik	69.617 N	162.300 E	1950–99	24 Chetyrehstolbovoi	70.633 N	162.483 E	1951–93
25 Aion	69.933 N	167.983 E	1954–99	26 Pevek[a]	69.700 N	170.250 E	1950–06
27 Billingsa	69.883 N	175.767 E	1953–94	28 Mys Shmidta	68.900 N	179.367 W	1950–93
29 Vrangelia	70.983 N	178.483 W	1950–99	30 Vankarem	67.833 N	175.833 W	1950–99

[a]Nine stations with longest records, see Figures 1 and 2.

model improvements by introducing neglected effects and mechanisms important for SL variability.

2. Observational Data Description

[5] The SL data in the Siberian Seas are described by *Proshutinsky et al.* [2004]. Instrumental measurements of SL in the Arctic Seas began in the 1920s and 1930s. Stationary SL observations first began in the Kara Sea (Dickson Island) in 1933, in the Laptev Sea (Tiksi Bay) in 1934, in the Chukchi Sea (Cape Schmidt) in 1935, and in the East Siberian Sea (Ambarchik Bay) in 1939. In the mid 1980s, 71 stations were involved in the SL observational program. As a result of economic problems in Russia, many stations were closed in the 1990s, so that at present there are only 18 stations operating in the Siberian Seas. Among these 18 stations only the 9 stations shown in Table 1 and Figure 2 have records without seasonal gaps for the entire period of 1954–2006. SL observations were conducted according to the *Manual for Stations and Gauges of the Hydrometeorological Service* [1968]. The observations based upon manual readings were carried out four times a day with an accuracy of 1 cm. Automated tide gauge stations equipped with tide-gauge recorders (see Table 1 for their locations in *Proshutinsky et al.* [2004]) have a sampling frequency of 1 hour and an accuracy of 1 cm. Monthly data quality control includes both visual data control and statistical control. Observations at some stations were at different locations in summer and winter; some of which were interrupted during replacement. Much of the SL data collected before 1949–1950 cannot be used for analysis because of the absence of a reliable geodetic survey. All stations shown in Table 1 from *Proshutinsky et al.* [2004] have one or more geodetic benchmarks installed on stable ground. Periodic geodetic surveys were made to each gauge to determine if any vertical changes in the gauge mount occurred. If a change in the SL gauge mount occurred, an adjustment was made. The SL data used in this paper are relative to benchmarks in solid rock and are corrected for glacial isostatic adjustment (see *Proshutinsky et al.* [2004] for details).

[6] For this study, only 30 stations are used (Table 1 and Figure 2). These stations are most representative for purposes of model validation and do not have local features in the SL regimes. Local SL variability can be caused by unusually narrow bays or river deltas, by extreme river discharge, or by very shallow waters which may not be reproduced by regional Arctic models. The time series of SL variability generally cover the period between 1948 and 2000, but temporal coverage differs significantly from station to station. For model intercomparison a common period from 1960 through 1980 is chosen, but the period from 1960 through 2000 is used for the analysis of interannual variability. These periods were chosen because some AOMIP models have simulated data only after 1959.

3. Participating Models and Forcing

[7] This paper analyzes monthly SSH outputs from five AOMIP models with free surfaces, namely: (1) The Naval Postgraduate School regional Arctic Ocean model (NPS); (2) The Goddard Space Flight Center regional Arctic Ocean Model with course resolution (GSFC1); (3) The Goddard Space Flight Center regional Arctic Ocean Model with high resolution (GSFC2); (4) The Los Alamos global ocean model (LANL); (5) The University of Washington regional Arctic Ocean model (UW).

[8] The major model configurations and parameters are shown in Table 2. In addition, a 2-D coupled ice-ocean barotropic model (hereafter, 2-D model) developed by *Proshutinsky* [1993] was used to investigate the role of bathymetry, river runoff, fast ice, and inverted barometer effects (IBE). All models listed above have a barotropic ocean dynamics module similar to Proshutinsky's 2-D ocean model module. The 2-D model does not have thermodynamics; sea ice thickness is fixed and corresponds to mean climatic conditions [*Proshutinsky and Johnson*, 1997], and sea ice concentration is prescribed monthly from observations. This model also includes fast ice, established on October 1, for which sea ice motion is prohibited in the regions with depths shallower than 25 m. This limitation acts until May 1 when it is suggested that the fast ice becomes pack ice or disappears according to observed sea ice concentrations. The model's domain is based on a stereographic map projection with a horizontal resolution of 55.5 km and includes the Bering Sea in the Arctic's

Table 2. Model Configuration and Parameters

Characteristic	GSFC1	GSFC2	LANL	NPS	UW	2-D
Domain[a]	regional	regional	global	regional	regional	regional
Vertical coordinate	σ	σ	z	z	z	–
Bering Strait	restored	restored	open	closed	open	open
Resolution[b]	~0.8°	~0.4°	~0.4°	18 km	~22 km	55.5 km
Vertical levels	22	26	40	30	25	1
Minimum depth	50 m	50 m	20 m	45 m	50 m	5 m
Ocean δt	1080 s	720 s	1800 s	1200 s	720 s	120 s
Equation of state	Mellor (1991)	Mellor (1991)	UNESCO[c]	UNESCO[d]	UNESCO	—
Hor. friction	Smagorinsky	Smagorinsky	biharmonic	biharmonic	biharmonic	10^9 cm^2/s
Vertical mixing	Mellor-Yamada (1982)	Mellor-Yamada (1982)	KPP[e]	PP[f]	KPP[e]	—
Tracer advection	Lin et al. (1994)	Lin et al. (1994)	3rd order upwind	centered difference	centered difference	centered difference
Momentum advection	centered difference	centered difference	centered difference	PV conserving	centered difference	centered difference

[a]Regional domains generally include the Arctic Ocean and North Atlantic.
[b]Resolution in degrees refers to the rotated grids used by regional models. LANL and UW use a nonuniform displaced pole grids with the North Pole singularity in North America (LANL) or Greenland (UW).
[c]*Jackett and McDougall* [1995].
[d]*Parsons* [1995].
[e]*Large et al.* [1994].
[f]*Pacanowski and Philander* [1981].

Pacific sector. In the Atlantic Ocean, the model's boundary is located approximately along 55°N. The model was run under coordinated AOMIP forcing fields.

[9] All 3-D model specifications are outlined by *Holloway et al.* [2007]. Some specifics about 3-D models analyzed in this paper are briefly described below.

3.1. AOMIP Coordinated Model Forcing

[10] The coordinated AOMIP experiment was designed to ensure an accurate intercomparison experiment, and to eliminate ambiguities in interpretation of model results. The major idea of this experiment was to test each model's behavior under common initial and boundary conditions and under common model forcing. The conditions of this experiment are outlined in details at the AOMIP website and summarized by *Hunke and Holland* [2007].

3.2. NPS Model

[11] The NPS model is based on the Parallel Ocean Program (POP) [*Smith et al.*, 1992; *Smith and Gent*, 2002] adapted to the Pan-Arctic region. POP is a member of the Bryan-Cox class of z- coordinate ocean models with an implicit free surface. In the NPS model this ocean module is coupled to a parallel version of the *Hibler* [1979] dynamic-thermodynamic sea ice model [*Maslowski et al.*, 2000; *Zhang et al.*, 1999].

[12] The model domain extends from Bering Strait, over the Arctic Ocean, into the sub-polar seas and the North Atlantic to approximately 45°N. All model boundaries are solid (i.e. Bering Strait is closed) and no mass flux is allowed through them. Surface temperature and salinity are restored toward monthly climatology on timescales of 365 and 120 days, respectively. The grid is relatively fine (18 km and 30 vertical levels).

3.3. GSFC Models

[13] Two GSFC model results are analyzed and discussed in this paper: GSFC1 (coarse resolution = 0.7° × 0.9°) and GSFC2 (finer resolution = 0.33° × 0.4°) models. Both are based on the Princeton Ocean Model (POM) with explicit free surface. The basic model employed at GSFC is a sigma coordinate model [*Blumberg and Mellor*, 1987]. Both models are coupled to a dynamic- thermodynamic ice model [*Häkkinen and Mellor*, 1992; *Häkkinen and Geiger*, 2000] and use AOMIP coordinated model run forcing specifications except the following: both GSFC models use P-E from *Rasmusson and Mo* [1996], and the Sellers formula as in *Parkinson and Washington* [1979] for short wave radiation instead of AOMIP recommendations; the GSFC2 model uses NCEP wind instead of AOMIP recommended wind forcing. Transport at the open boundaries is defined by an inflow of 0.8 Sv through Bering Strait, which equals the amount that exits through the model's southern boundary at approximately 15°S. No restoring is used in the GSFC models. With these exceptions, the GSFC1 model follows all AOMIP specifications. The GSFC2 model results are from a run that was re-initiated from 45 years of spin-up using daily NCEP Reanalysis data. Other GSFC2 differences from the GSFC1 model include decreased lateral friction and better resolved topography.

[14] In many cases we do not show results from the coarse resolution model, and "GSFC" refers to results from the high resolution model.

3.4. LANL Model

[15] The LANL global ocean-ice model is fully described by *Hunke and Holland* [2007]. It is based on the POP, version 2.0 model, coupled with the LANL sea ice model [*Hunke and Lipscomb*, 2004]. The model forcing is specified as recommended by AOMIP. The ice and ocean models are discretized for nonuniform, orthogonal grids with a 0.4° global mesh with 40 vertical ocean levels.

3.5. UW Model

[16] The UW model is a variant of the Global Parallel Ocean and Ice Model (POIM) [*Zhang and Rothrock*, 2003]. This is a so called super regional POIM with a southern open boundary along the latitude of 45°N. The POIM couples the POP with a sea ice model of *Zhang and Rothrock* [2003].

[17] The mean model horizontal resolution is 22 km for the Arctic, Barents, and GIN (Greenland-Iceland-Norwegian) seas, and Baffin Bay. The model was driven by daily NCEP/NCAR reanalysis data. The calculations of surface

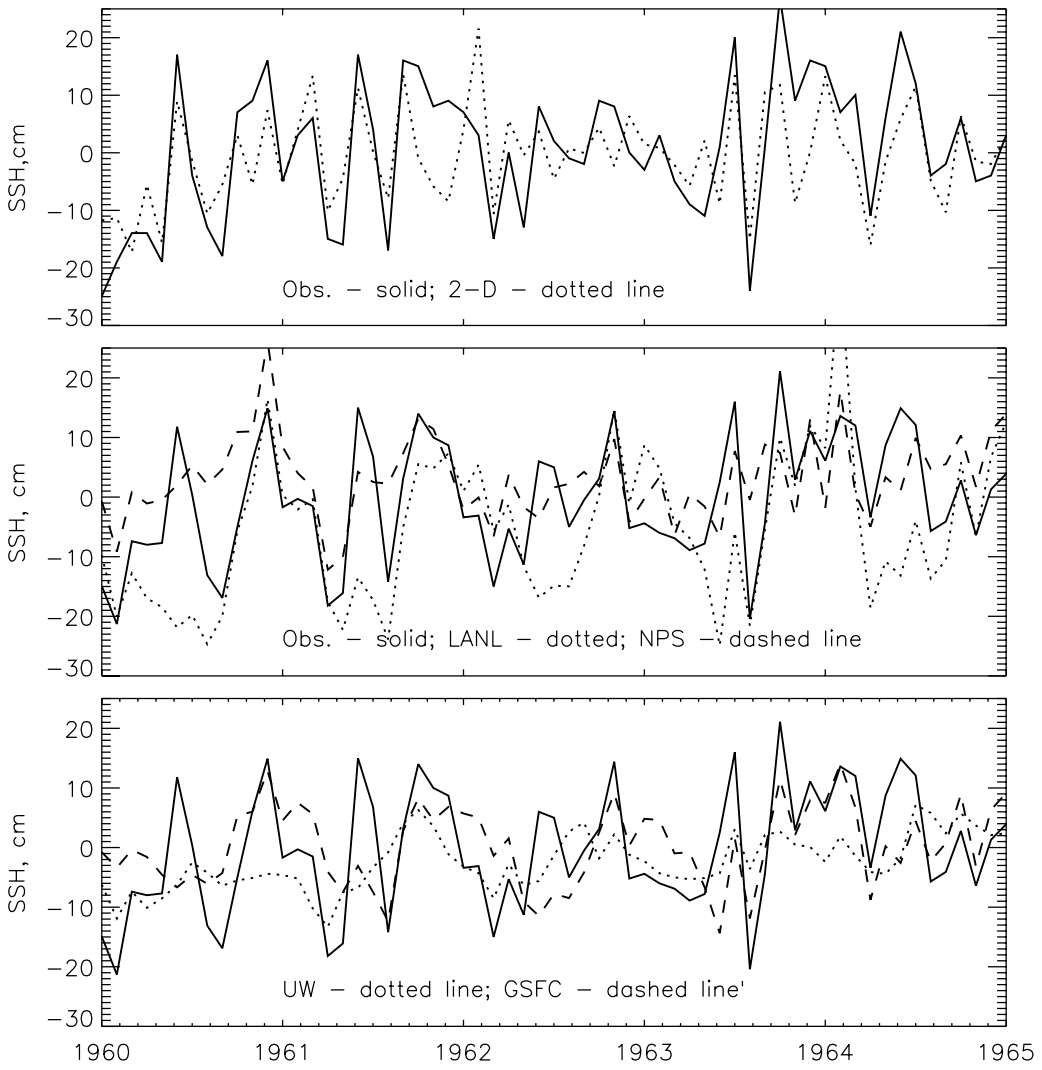

Figure 3a. Results of SL simulations for station Dikson in the Kara Sea. Note that the observed data in the upper panel are not corrected for the inverted barometer effect. Correlation between observations and simulations is shown in Table 3.

momentum and radiation fluxes follow *Zhang and Rothrock* [2003] and differ from the specifications for the AOMIP coordinated runs. No climate restoring is allowed. The open boundary conditions are from a global POIM driven also by the reanalysis. Additional information about some of the ocean parameters can be found in *Zhang and Steele* [2007].

3.6. Modeled Data

[18] There are some important features and differences among the models and their forcing which must be noted during the intercomparison procedure. First, the analyzed 3-D models neglect IBE (atmospheric loading) so their simulated SSH do not vary due to changes in atmospheric pressure over the Arctic Ocean. This is a relatively serious problem because seasonal variability of SLP is responsible for significant SL oscillations. Figure 1 shows that the SLP is an important factor in both SL variability and variability of the annual AO index. Fortunately, the IBE may be subtracted from the observations for seasonal and long-term variability studies by assuming that 1 hPa of the SLP change corresponds to −1 cm in the sea surface change. Validation of all models except the 2-D model was carried out against observational data corrected for the IBE. To validate the models, SSH were extracted from the original model results at grid points corresponding to the station locations. Thirty stations were used for comparison over the 252 month period from 1960–1980 (Figure 2). The observational data are represented by relative SLs (anomalies from climatologic mean). In order to make data comparable, all simulated data sets are also represented as anomalies from model climatologic means.

4. Model Results

[19] Three major statistical parameters were used to characterize model results, namely the root mean square error (RMSE), the standard deviation (STD) and the correlation coefficient (COR) between the observed and simulated time series of monthly SSH at station locations. Figures 3a and 3b show a typical result of model intercomparison. The statistics are presented in Table 3 and Figure 4. Based on statistical parameters it is interesting that the

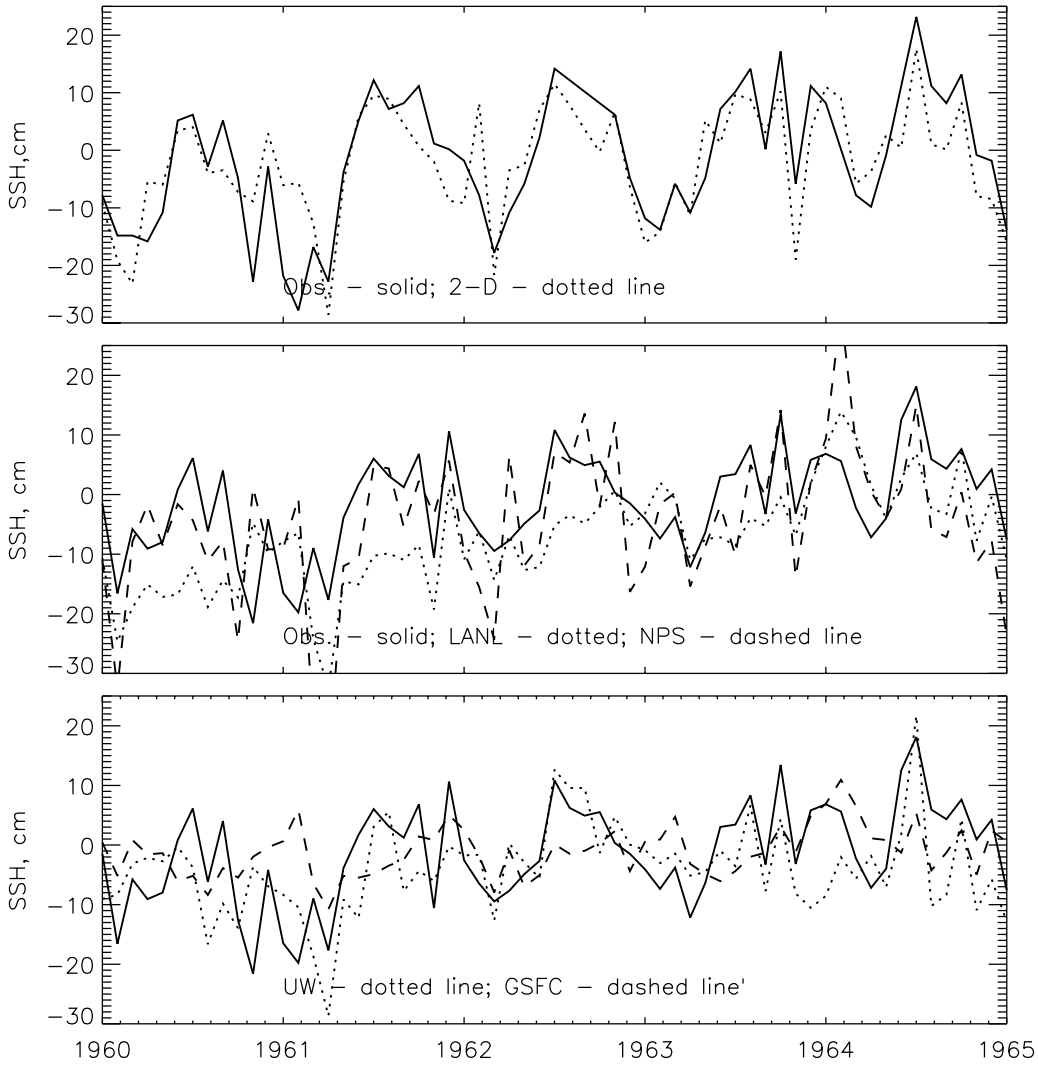

Figure 3b. Results of SL simulations for station Vrangelia in the Chukchi Sea. Note that the observed data in the upper panel are not corrected for the inverted barometer effect. Correlation between observations and simulations is shown in Table 3.

simplest 2-D barotropic model provides better results than all other models. Reasons for this will be discussed in section 5.

4.1. Seasonal Variability

[20] The seasonal variability of most Arctic environmental parameters is very large [*Polyakov et al.*, 1999]. SL data reflects this very well. The seasonal changes in Arctic SL have been discussed in many publications [*Dvorkin et al.*, 1978, 1983, 2000; *Pavlov and Pavlov*, 1999; *Proshutinsky*, 1978, 1993; *Proshutinsky et al.*, 2001, 2004; *Vorobyov et al.*, 2000] and the IBE, wind regime, river runoff, and steric effects associated with water temperature and salinity change have been identified as major factors influencing SL seasonal cycle. Figure 5 shows results of simulated seasonal SL variability where the simulated data were averaged for 30 stations to produce a "mean" seasonal cycle for 21 years, and correlations and errors of these composite time series were calculated for each model. Observations show that there is a maximum in SL in June and July depending on station location which is associated with an increase in river runoff (maximum in June), a decrease in the atmospheric pressure (IBE) with minimum in July or August, and to a lesser degree, an increase of water temperature because of solar radiation (maximum in late August). The second maximum is usually observed in October–just before fast ice formation. With intensifying storm activity, precipitation increases and the wind regime becomes more cyclonic along coastlines, causing SL to rise in September and October. In April, the absolute minimum in SL seasonal cycle is observed when SLP reaches its maximum (SL decreases due to atmospheric loading), water temperature is at the freezing point, water is at its most saline, fast ice extent is maximal, and river runoff is minimal. All models capture this SL minimum in winter, with differing degrees of accuracy, but they all miss the SL maximum in July. Instead they have only one maximum in autumn, with SL gradually increasing from its minimum in April to maximum in October–December. The UW model shows an unusual seasonal pattern with one maximum in August.

Table 3. Model Validation Results for 1960–1980

	COR					RMSE				
Tide Gauge	NPS	UW	GSFC	LANL	2-D	NPS	UW	GSFC	LANL	2-D
Bolvanskii Nos	0.31	0.05	0.49	0.32	0.56		10.0	11.5	9.3	10.0
Amderma	0.51	0.15	0.34	0.09	0.60	6.5	8.3	6.8	9.1	8.5
Russkaia Gavan'	0.50	0.14	0.58	0.31	0.60	8.9	11.1	8.4	10.7	10.3
Harasavei	0.47	0.24	0.50	0.42	0.66	8.9	10.2	8.7	10.9	10.0
Zhelania	0.47	0.11	0.45	0.38	0.60	12.5	14.2	12.5	14.0	13.6
Dikson	0.60	0.40	0.54	0.47	0.71	9.9	11.4	10.5	13.1	11.2
Uedinenii	0.13	0.01	0.46	0.31	0.58	9.9	10.0	7.6	9.8	9.0
Izvestia CIK	0.44	0.20	0.59	0.55	0.69	9.3	9.7	7.8	9.4	9.2
Sterlegova	0.64	0.35	0.61	0.60	0.69	9.9	12.0	10.0	11.9	11.6
Isachenko	0.18	0.22	0.25	0.31	0.65	9.8	9.2	8.7	10.3	9.1
Golomianyi	0.22	−0.20	0.23	0.09	0.57	7.2	9.6	7.2	9.7	8.9
Pravdy	0.54	0.31	0.63	0.58	0.70	10.4	11.0	8.8	11.3	9.9
Fedorova	0.47	0.22	0.39	0.39	0.70	8.5	8.7	7.8	10.0	8.6
Andreia	0.39	0.39	0.32	0.46	0.59	9.4	9.3	9.5	10.0	10.1
Preobrazhenia	0.46	0.47	0.54	0.52	0.61	9.6	9.4	9.2	9.6	10.4
Dunai	0.49	0.55	0.42	0.47	0.70	10.4	9.3	10.1	11.1	9.9
Tiksi	0.59	0.61	0.44	0.49	0.77	9.8	10.0	9.7	10.9	8.7
Muostakh	0.48	0.53	0.38	0.43	0.74	13.5	13.0	13.7	14.1	10.3
Kotel'nyi	0.58	0.53	0.49	0.41	0.71	10.0	9.6	9.9	12.4	10.4
Sannikova	0.59	0.46	0.20	0.35	0.73	9.9	10.1	11.1	12.3	9.9
Kigiliakh	0.62	0.59	0.37	0.57	0.76	9.9	10.0	10.3	10.0	9.2
Shalaurova	0.48	0.54	0.42	0.54	0.72	11.9	10.9	11.0	11.3	10.6
Ambarchik	0.43	0.44	0.37	0.37	0.66	15.0	12.9	13.5	16.3	12.8
Chetyhrehstolbovoi	0.67	0.26	0.52	0.60	0.74	12.6	9.8	11.3	12.5	10.7
Aion	0.60	0.62	0.48	0.53	0.72	12.3	9.8	11.5	13.4	10.2
Pevek	0.65	0.74	0.49	0.61	0.76	11.9	8.7	11.4	11.9	9.8
Billingsa	0.59	0.62	0.48	0.55	0.72	13.4	9.8	11.1	13.1	10.3
Mys Shmidta	0.63	0.64	0.51	0.52	0.70	12.7	9.8	11.0	13.0	10.7
Vrangelia	0.54	0.68	0.41	0.50	0.71	11.3	7.3	8.4	9.2	8.4
Vankarem	0.63	0.65	0.53	0.57	0.69	13.0	10.6	12.5	12.2	11.7
Mean	**0.49**	**0.40**	**0.45**	**0.44**	**0.68**	**10.6**	**10.2**	**10.0**	**11.5**	**10.0**

4.2. Interannual Variability and Trends

[21] The interannual variability and trends were investigated for the period 1960–2000 common to all models. Figure 6 shows 1960–2000 mean SSH for all models and EOF analyses of SSH variability. To carry out these analyses, monthly model data from the original model grids were linearly interpolated onto a common grid and detrended. The mean SSH fields differ significantly from model to model and reflect differences in many model parameters such as water temperature and salinity, circulation, and sea ice conditions discussed in the other papers presented in this volume [*Holloway et al.*, 2007; *Karcher et al.*, 2007; *Zhang and Steele*, 2007]. For example, the elevated sea surface height in the center of the Beaufort Gyre is a good indicator of the thermohaline water structure in this region (low salinity), clockwise circulation and a large freshwater content. In the NPS model, this feature dominates the entire Canada Basin. The other models show some signs of the Beaufort Gyre but it is significantly less pronounced than in the NPS model. Interestingly, all 3-D models have a very well pronounced Beaufort Gyre after their initialization in the early years of the simulation (not shown). Later, this feature gradually disappears, likely due to enhanced mixing of upper layers with deeper ocean layers (see discussions in *Golubeva and Platov* [2007] and *Zhang and Steele* [2007]). It is likely that mixing problems result in a salinity increase in the upper layers of the Beaufort Gyre, weakening and smoothing the gyre's dome-shaped SSH structure. For example, the restoring procedure applied in the NPS model probably improves this situation by supplying climatological salinity into the upper ocean. Indeed, while the other analyzed models did not restore or stopped restoring after 10 years of simulation, the NPS model experiment included restoring during the entire period of simulation.

[22] The 2-D model has negative SSH instead of positive in the Beaufort Gyre because it does not include baroclinic effects and takes into account atmospheric loading. In the 2-D barotropic model, wind stress does not provide significant SL elevation under the Beaufort high because the ocean is too deep (see Figure 7 showing components of SSH generated by Bering Strait inflow, wind and atmospheric loading forcing) and the only important barotropic factors responsible for SSH variability in this region are the IBE (leading to the SSH depression under the atmospheric high pressure) and the Bering Strait inflow, which determines the major barotropic circulation in the Chukchi Sea and the water through-flow from the Bering Strait to the North Atlantic along the Alaskan and Greenland coastlines.

[23] Theoretically, under atmospheric loading alone (Figure 7c) we should not observe any water motions in the region because SLP gradients have to be balanced by SSH gradients. But in the case of the Arctic Ocean with the narrow and shallow Bering Strait, the ocean is not fully adjusted to SLP forcing and there is a current in Bering Strait associated with atmospheric loading even after 1 month of forcing. This common problem with shallow water and narrow straits in the ocean dynamics when atmospheric loading is not fully compensated by IBE has been mentioned in many publications [e.g., *Carrere and Lyard*, 2003; *Yoshida and Hirose*, 2006; *Vinogradova et al.*, 2007].

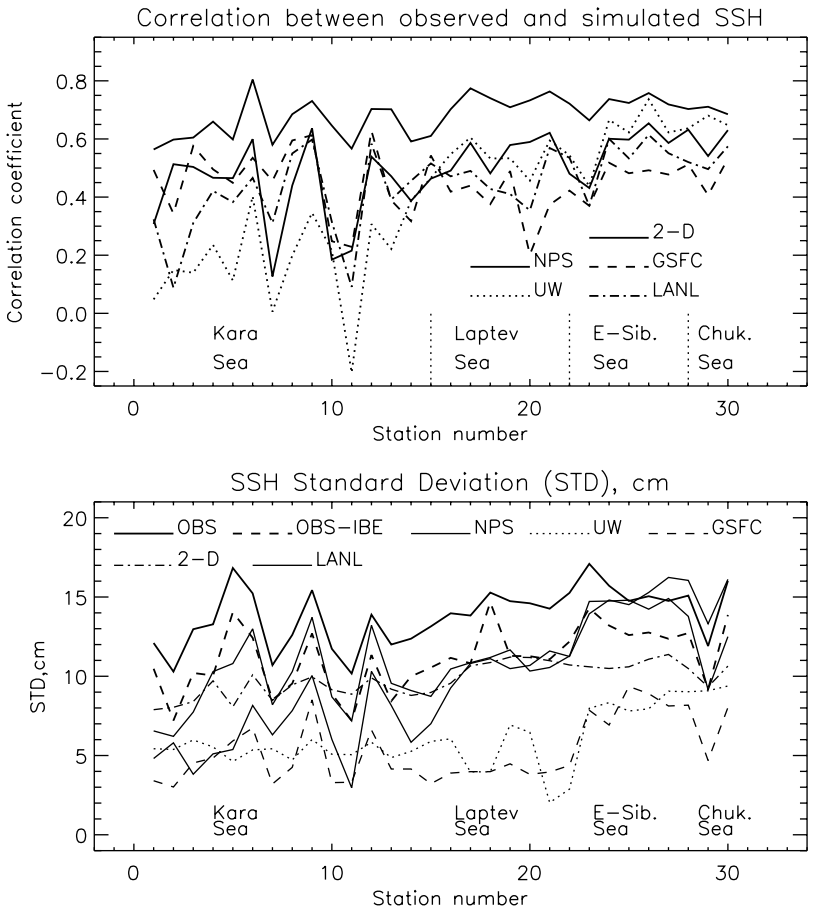

Figure 4. Statistical parameters characterizing simulation results. Upper panel shows correlation coefficients between observed and simulated SL at 30 tide gauges along the Siberian coastline. Lower panel shows standard deviations of the observed SSH (Obs.), observed SSH corrected for the inverted barometer effect, and simulated SSH from the 2-D and AOMIP models.

[24] In Figure 6, the Bering Strait inflow also is visible in all 3-D models (increased gradients in SSH), except the NPS model where Bering Strait is closed.

[25] The first EOF mode (Figure 6) shows that the maximum change occurs in SL fields in the Canada basin and GIN (Greenland, Iceland and Norwegian seas) Sea region. In the LANL model, the first mode describes 34% of SSH variability and during 1960–1970 it supports positive anomalies of SL in the center of the BG. After 1970, this anomaly changes sign and the circulation anomaly in the BG becomes cyclonic. After 1992 the system returns to its initial state.

[26] In general, the behavior of UW, GSFC, NPS and 2-D model EOF coefficients are similar. The decadal signals in these models resemble the AO index (dashed line in bottom right panel of Figure 6) indicating that it is likely that wind-driven forcing dominates in these models.

[27] Figure 8 presents smoothed annual mean composite time series for all models and their correlation with the AO and observational data. SSH correlates well with the AO index for all models, but the magnitudes of variability are relatively small in the GSFC and NPS models. The 2-D model has a bit higher variability, influenced mainly by the IBE. The variability of the LANL model is "contaminated" by a large positive trend (not shown), but detrended data shows excellent agreement with the AO index, and the magnitude of variability agrees with the observational time series better than the other models. Linear trends for 5-year running mean time series (1962–1998) are shown in the upper left corner of Figure 8. The observed trend for 9 stations which have records for 1962–1998 is 0.171 cm/yr. The 2-D and NPS models have trends of 0.108 and 0.052 cm/yr, respectively. The GSFC coarse and high resolution models have 0.078 and 0.006 cm/yr trends, respectively. The LANL model's trend is positive and is 1.02 cm/yr for 1962–1998 which, as speculated above, is because of the model drift. After data detrending for the entire period of simulation, the LANL SSH trend for 1962–1998 is 0.027 cm/yr. The mean trend for all models results is 0.072 cm/yr which is less than the observed trend. This estimate may not make sense because there is a significant underestimation of the interannual variability in all models except the UW and LANL models, and the last one overestimates this trend. The best results were obtained by the UW model (0.163 cm/yr). Figure 9 shows the spatial variability of SSH trends for the models. The UW, GSFC1 (not shown), LANL, and 2–D models show positive trends along all coastlines, but the GSFC2 model and the NPS model show that some coastal

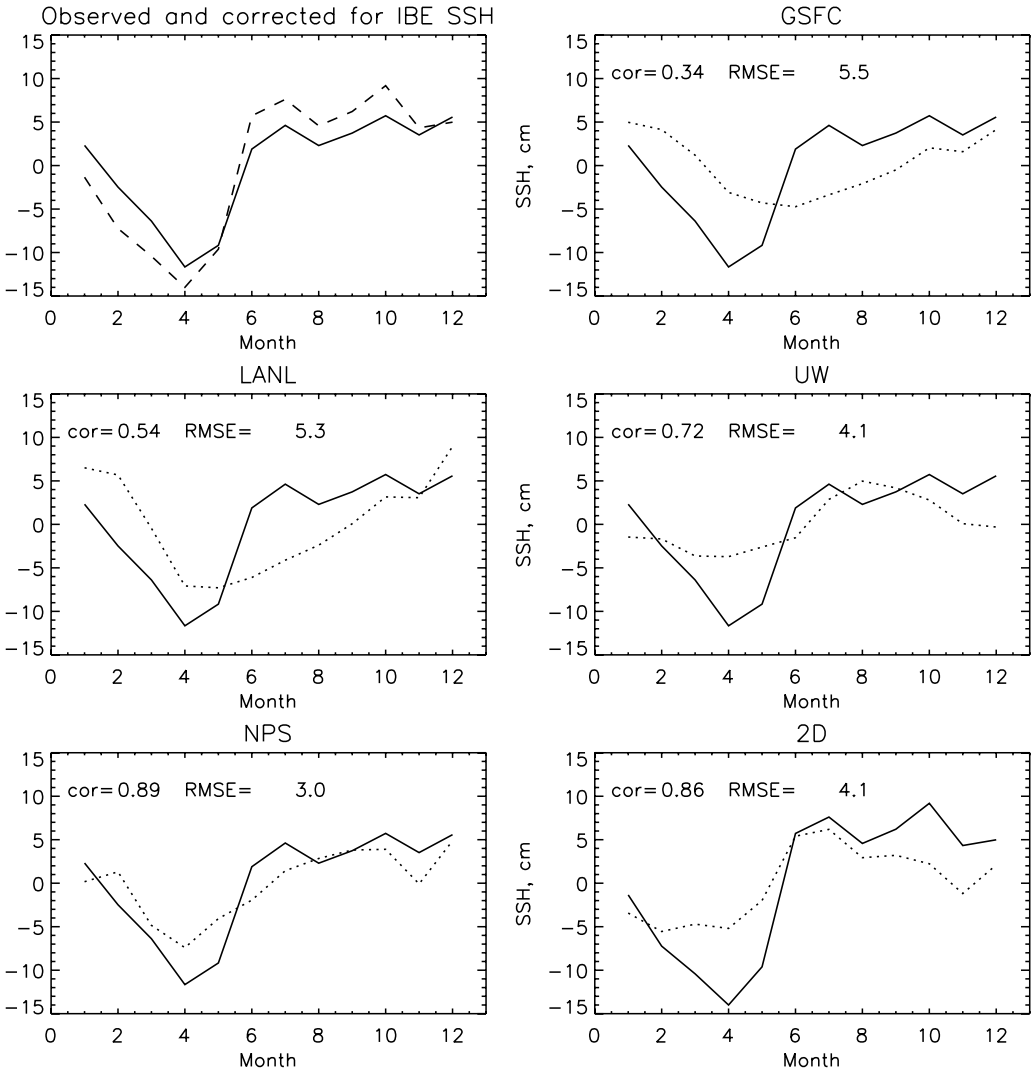

Figure 5. Seasonal variability of SL averaged for 30 stations for a mean seasonal cycle for 1960–1980 and shown in Table 1 and Figure 2. Upper left panel shows observed SSH (dashed line) and SSH corrected for inverted barometer effect (solid line). In remaining panels, solid lines depict observations corrected for the inverted barometer effect (except 2-D model results), and dotted lines show model results. Numbers in figures show correlations between observed and simulated time series and RMSE (cm).

regions have negative SSH trends. This contradicts the observational data from coastal tide gauges. All 3–D models have a negative SL trend in the central Arctic Basin which may be associated with increasing salinity in the Atlantic layer.

5. Discussion: Causes of Model Discrepancies

[28] In order to understand why the 3–D models do not reproduce observed SL changes well, different factors influencing model solutions at different timescales are analyzed. First, some obvious problems are discussed without long-term 3-D model runs, then other speculations and conditions are added.

5.1. Bathymetry Resolution

[29] One of the important factors limiting model performance is its resolution. The NPS, LANL, GSFC1, GSFC2, UW and 2-D models have horizontal resolutions of approximately 18 km, 9–20 km, 70 km, 35 km, 5–32 km, and 55 km, respectively. Comparing 3-D model results shown in Table 3 one sees that the NPS model with a horizontal resolution of 18 km better agrees with observations than other 3-D models (correlation coefficient between simulated and observed monthly SL time series is 0.49 versus 0.37–0.45 coefficients of other models). The GSFC1 model with a horizontal resolution of approximately 70 km has the lowest correlation with observations. Regarding other observational parameters, experiments with horizontal model resolution were carried out by *Golubeva and Platov* [2007] showing that the increase of horizontal resolution improves model results.

[30] Another factor related to the resolution is the minimum ocean depth allowed in the model (see Table 2). Resolution of the bathymetry, especially in the vast Arctic marginal shallow seas (that extend for hundreds of kilometers), is an important parameter because it determines SL

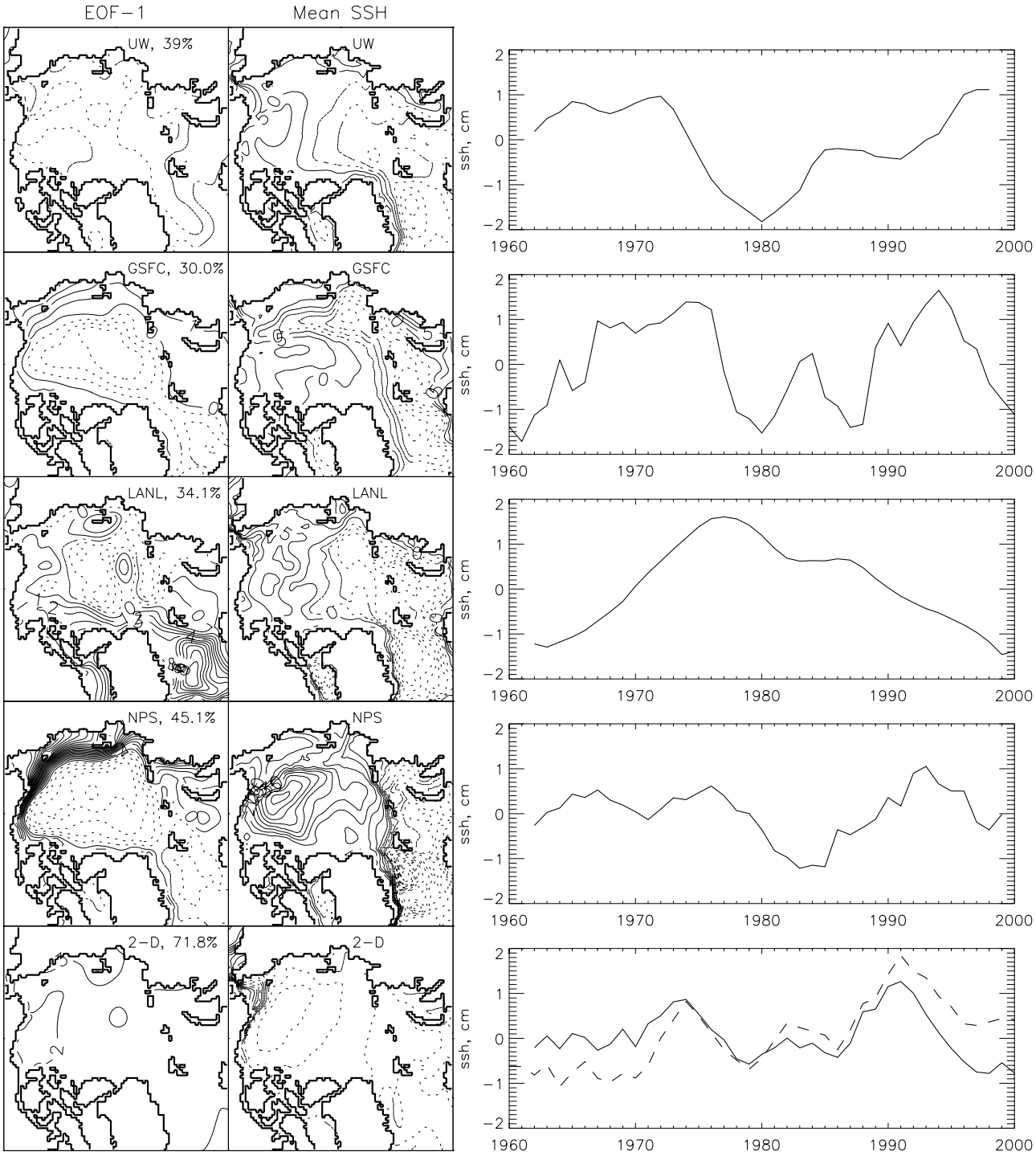

Figure 6. Sea surface height patterns for the first EOF mode (left panels) and mean SSH (middle panels) and time series of the first EOF mode coefficients (right panels) from the 5 models for 1960–2000. Numbers on the figures at left show the percent of variance described by mode 1. The AO index is plotted on the bottom right panel as a dashed line.

variations associated with wind, thermal and fresh water forcing and also the phase of long-waves generated in the ocean by the atmosphere. It is expected that an artificial increase of the minimum depth influences simulated SL heights due to wind forcing, but it also can have an effect on SL due to thermal effects and freshening. Unfortunately, we cannot show steric SL errors based on existing model outputs and no numerical experiments with 3-D models were carried out for these purposes. Comparing results shown in Table 3, one sees that in general (except the NPS model) the 3-D models with more realistic minimum depths perform better.

[31] In order to estimate the possible role which bathymetry plays in SL mechanical response to atmospheric forc-

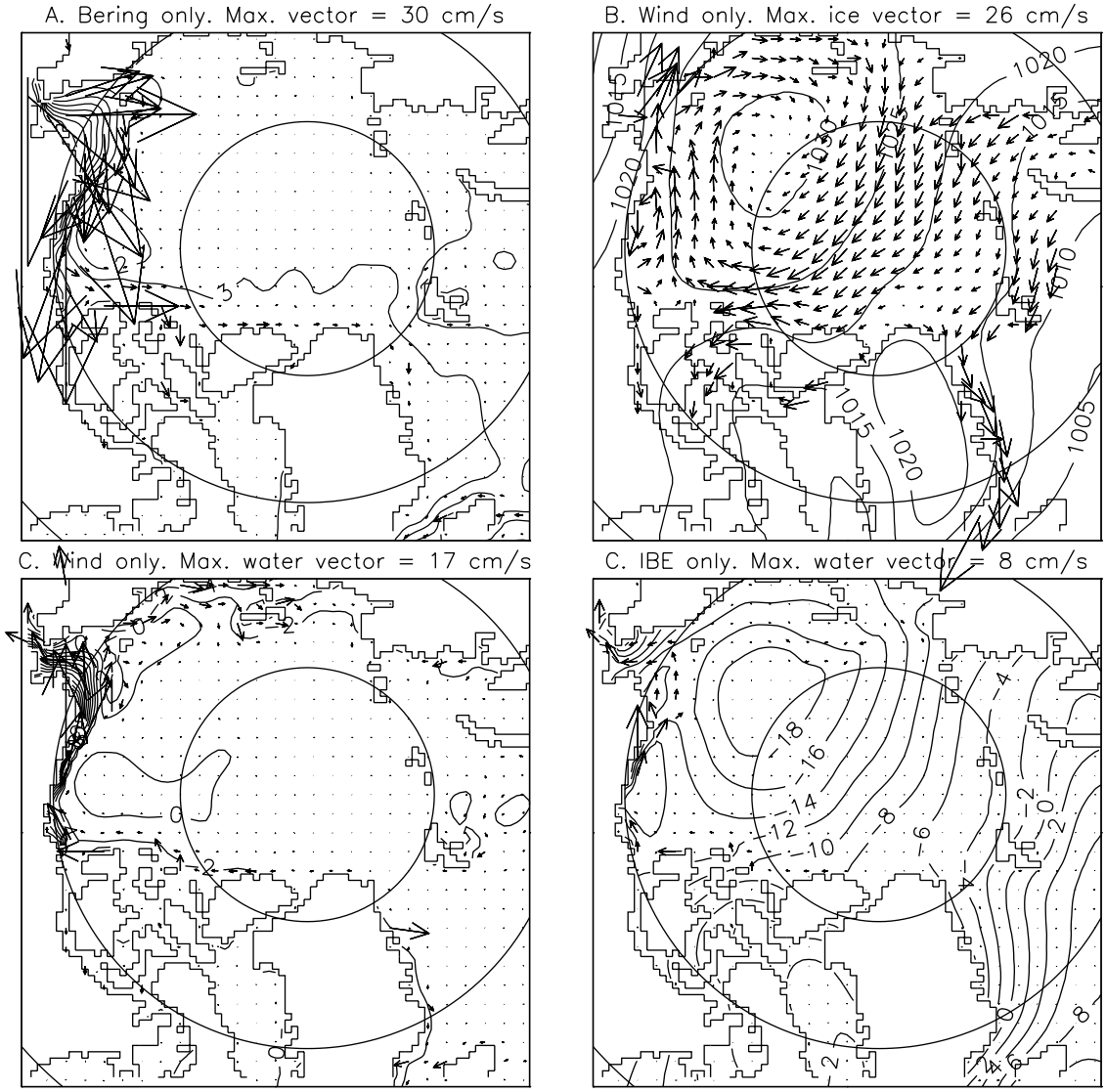

Figure 7. Components of sea surface heights from 2-D model results associated with: (a) only Bering Strait water inflow. SSH (contours: 0, 2, 3, 4, 10, 20, 30, 40 cm, etc.) and vertical mean water velocities are shown; (b) only wind forcing in January 1998. SLP distribution (hPa) and vectors of the simulated ice drift are shown; (c) only wind forcing. SSH (contour interval is 2 cm) and vertical mean water velocities; (d) only SLP forcing. SSH with 2 cm contour interval and vertical mean water velocities are plotted.

ing, the 2-D model was run with the minimum model depth artificially increased to 45 m. Figure 10 shows the major statistical parameters characterizing results of this experiment. There is a bias of approximately 2 cm in the Kara Sea (deepest marginal Arctic sea) with up to 6 cm in the East Siberian Sea (shallowest Arctic marginal sea) between two simulation results. This indicates that the strongest effect of the artificial deepening of the Arctic seas in the 3-D model should be expected in the East Siberian Sea, where its 45 m isobath lies approximately 200 km from the coastline. The correlation coefficient between these two data sets also shows that the minimum correlation is observed in the East Siberian Sea. The RMSE reaches 6 cm in the East Siberian and Chukchi Seas, approximately half of the SL standard deviation. Several experiments with minimum depths of 30, 20, and 10 m have shown that monthly simulated SSH time series for experiments with 5 m (control model run) and 10 m minimum depths are practically identical. Therefore we conclude that a minimum depth of less than or equal to 10 m in model domains could be recommended for improved SL model results.

5.2. River Discharge and a Role of Steric Effects

[32] River discharge is the second important factor influencing the ability of models to correctly represent seasonal variability of SSH, especially at coastal stations. Figure 11 shows seasonal variability of river runoff and SL at station Sopochnaia Karga on the Yenisei River in 1973. The river discharge at this station dominates all other factors. In the 2-D barotropic model the river discharge regulates SL variability very well and reproduces seasonal

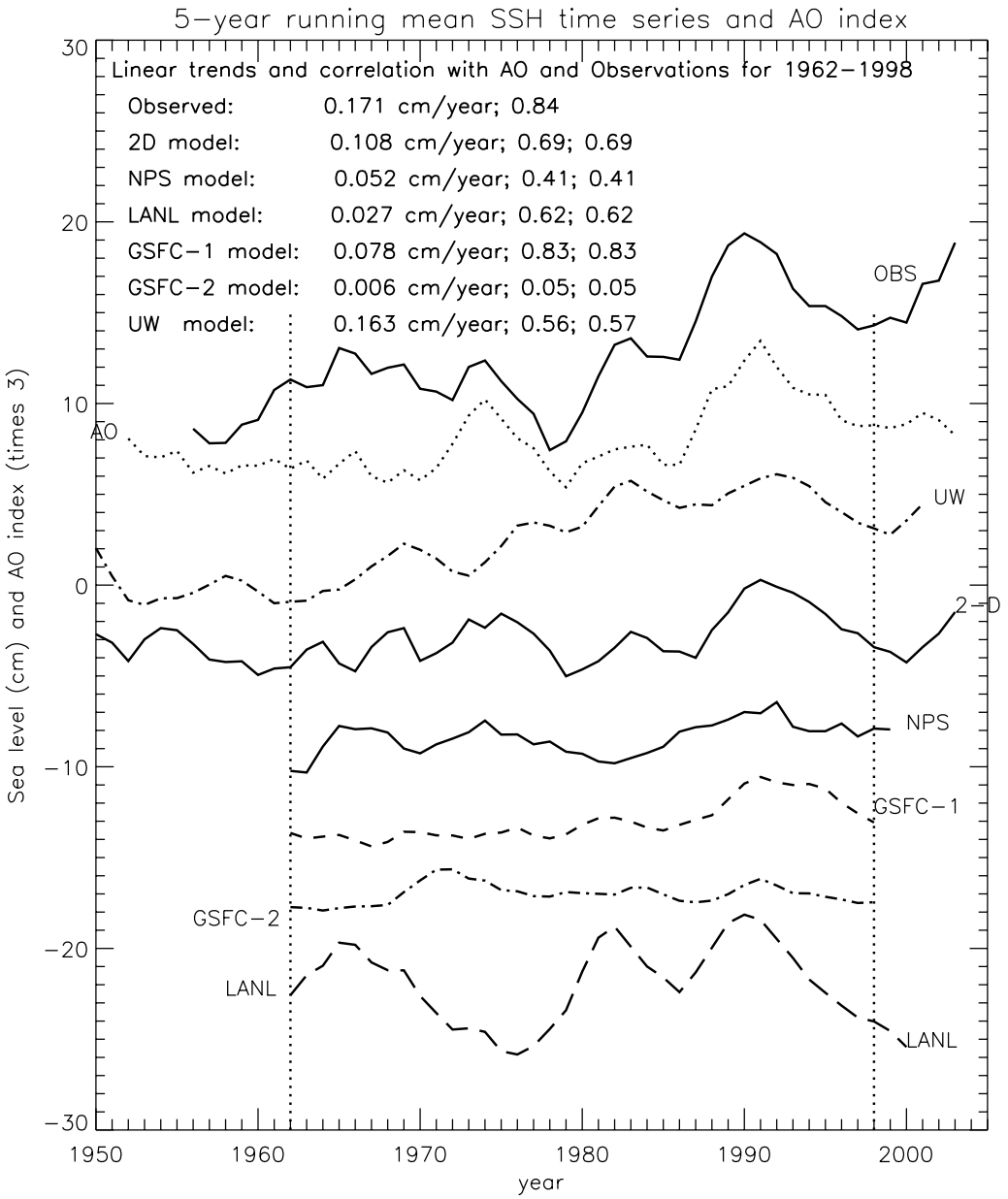

Figure 8. SSH 5-year running mean time series for all models. The data were averaged for 9 stations. Linear trends and correlation coefficients between simulated time series and AO and observed SL (OBS) are shown in left upper corner. Lines are shifted relative to 0 in order to better analyze differences. Note that LANL model time series was detrended to demonstrate decadal variability.

change similar to observations. Figure 12 shows statistical characteristics of SL variability with and without river runoff from the 2-D model results. There are significant differences in SL response between these two simulations indicating that even at the stations located far from river deltas, this factor plays an important role in SL variability. In the 3-D regional and global models analyzed here the river discharge is prescribed via salt fluxes ("salt sink") which mimic the freshening without actually adding any water volume. Figures 13a and 13b compare observations at two stations with SSH associated with water column expansion due to salinity and temperature change in the NPS model.

[33] The water thermal (*SterT*) and haline (*SterS*) contractions were calculated based on the following formulas [*Pattullo et al.*, 1955]:

$$SterT = \int_{z1}^{z2} \frac{1}{v}\frac{\partial v}{\partial T}\Delta T dz \qquad SterS = \int_{z1}^{z2} \frac{1}{v}\frac{\partial v}{\partial S}\Delta S dz$$

where v is specific volume, T and S are water temperature and salinity, z is depth, $z1$ and $z2$ are the lower and upper limits of depth of integration, and ΔT and ΔS are monthly water temperature and salinity anomalies at any particular model's depth level.

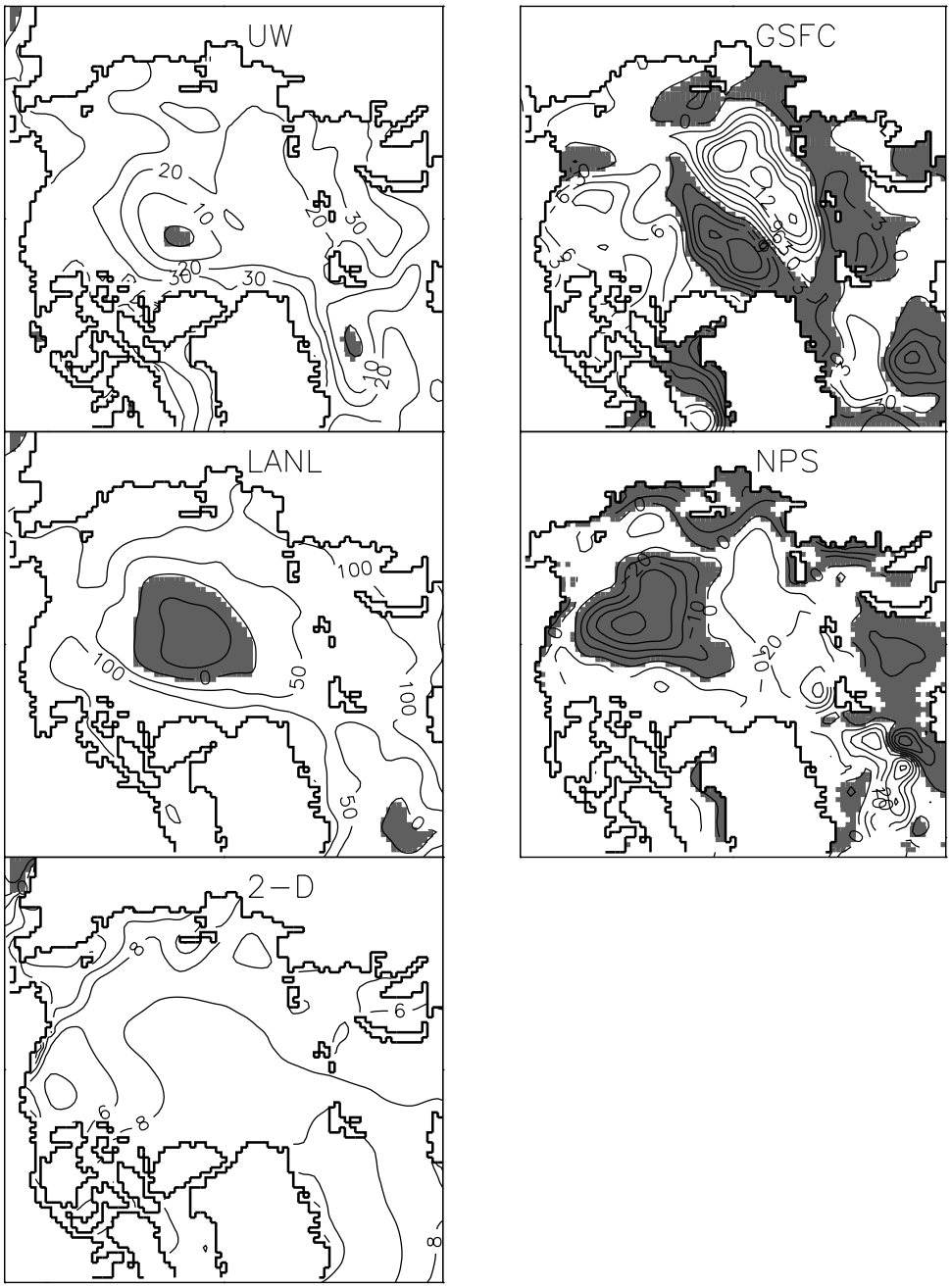

Figure 9. SL trends (cm per 100 years) from AOMIP models. Regions with negative trends are grey.

[34] Our calculations show that the NPS-modeled steric effects contribute substantially to the seasonal and interannual variability of simulated SL in the Kara and Laptev Seas (e.g., Figure 13a), with a reduction of inputs for the East Siberian and Chukchi Seas (Figure 13b). Figure 14 illustrates statistical parameters characterizing differences between the total simulated SSH of the NPS model and variability of SL simulated by NPS model water temperature and salinity changes. One sees that the role of SL variability associated with the steric effect in the NPS model gradually decreases from the Kara Sea (deepest sea) toward the East Siberian (shallowest) and the Chukchi Sea. In the Kara Sea, total SL variability is on the same order as the SL change due to steric effects, the correlation between the total SSH and steric SSH are higher than 0.6, and the ''errors'' are relatively small. In Figures 13a and 13b, we see that total SL from the NPS model decreases in winter (reduction of river runoff and increase of water salinity) and increases significantly in summer (maximum river runoff and freshening), in phase with the observed SSH. In the Laptev Sea (station Tiksi) the correlation between the total SSH and the SSH due to steric effects (read prescribed river runoff via prescribed salinity) is also high. SSH at other stations where there is no ''river runoff'' do not correlate well with steric effects. This is because the role of steric effects in the total SL variability is relatively small in the shallow East Siberian and Chukchi seas

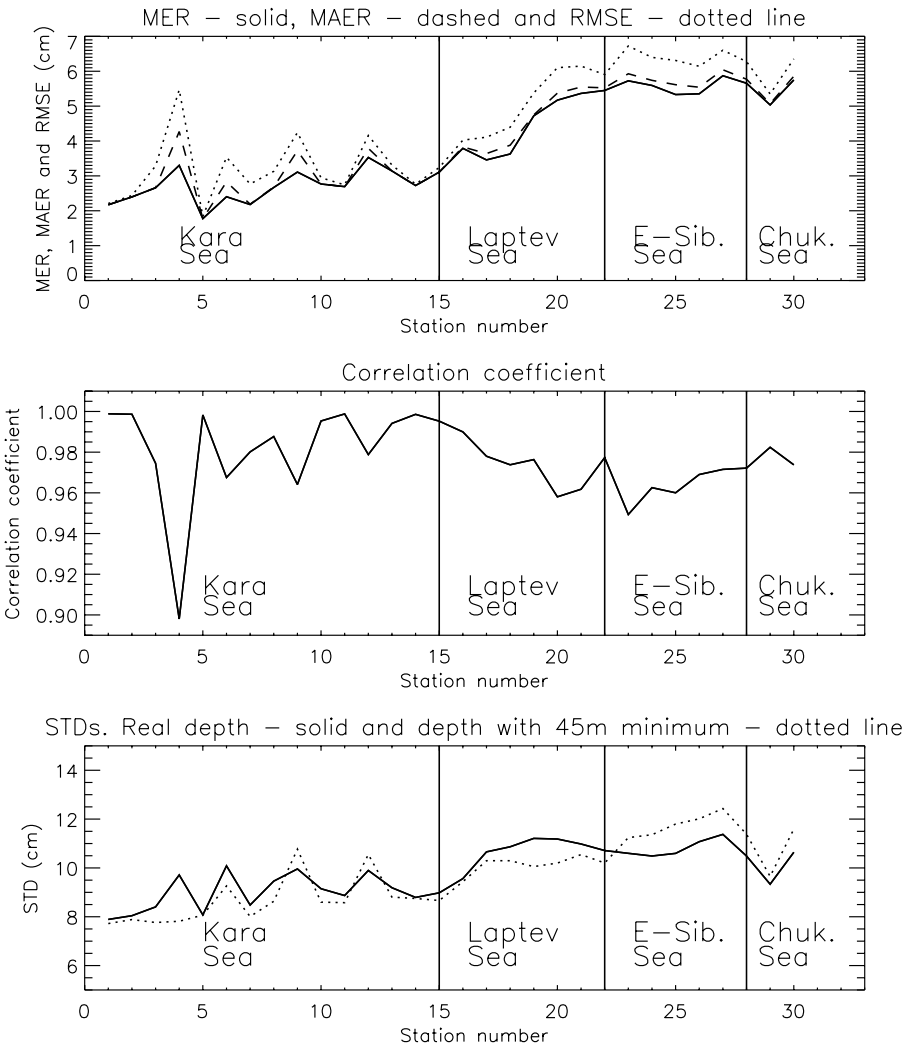

Figure 10. Statistical parameters characterizing results of "minimum depth" experiment. Upper panel shows mean error (MER), mean absolute error (MAER), and root mean square error (RMSE) associated with replacing "real" depths less than 45 m with the 45 m depth in the 2-D model. All other model parameters were left unchanged. Middle panel shows correlation coefficients for different stations between the control 2-D model run and a model run with the minimum depth of 45 m. Bottom panel shows SSH standard deviations (cm) for the control and experimental model run with minimum depth of 45 m.

(Figure 13b) and other factors like wind forcing, for example, prevail in SL seasonal variability.

[35] Both the absolute SSH and the role of steric effects in the western marginal seas can be significantly altered by highly variable Bering Strait water mass, temperature and salinity fluxes. This topic is further discussed in section 5.4.

5.3. Inverted Barometer Effect

[36] Corrections for atmospheric pressure variations are essential for studies of seasonal and interannual variability of mean SL. It is commonly accepted that these changes are not important for analysis of secular changes of SL because their long-term trends are small [*Woodworth et al.*, 1992]. However, for Arctic conditions where variability of SL pressure is substantial, this conclusion must be re-evaluated. For instance, *Walsh et al.* [1996] concluded that Arctic SL pressure data showed a significant decrease in the annual mean and changes were larger in the Central Arctic than anywhere else in the Northern Hemisphere.

[37] The relative contribution of several factors (wind stress, ice extent, and IBE) is different for different seasons. *Proshutinsky et al.* [2001] showed that during January–March, variability of observed SL at coastal stations is dominated by the IBE because vast areas of the Siberian Seas are covered by ice, damping the direct effect of wind forcing on water motion. Thus the relative importance of the IBE is regulated by the presence of fast or compact sea ice. It was also concluded that on average the IBE explains approximately 40%–60% of SL variability at seasonal and decadal timescales. *Proshutinsky et al.* [2004] found that the contribution of the inverse barometer effect to the Arctic Ocean SL rise during 1950–1989 is 0.056 cm/yr. This is the highest rate of SL rise among all estimates of this factor presented by *Intergovernmental Panel on Climate Change*

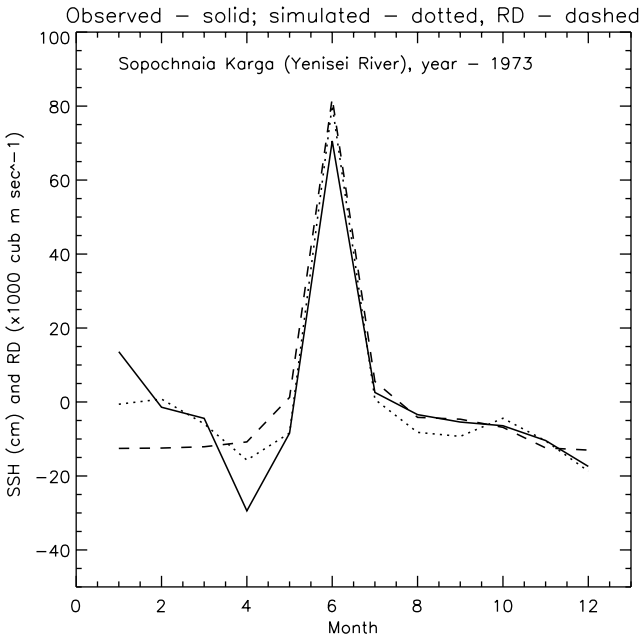

Figure 11. Observed (solid) and 2-D simulated (dotted) SSH at station Sopochnaya Karga (Yenisei River). Dashed line shows river discharge ($\times 10^3$ m^3 s^{-1}).

(*IPCC*) [2001] for various regions and is approximately 30% of the rate of SL change in the Arctic.

[38] Unfortunately, the ocean response to the IBE is still poorly accounted for by ocean models [*Wunsch and Stammer*, 1997], but there are several convincing attempts showing that this effect is important [e.g., *Carrere and Lyard*, 2003]. This is especially true for high latitude dynamics and shallow water regions, where corrections for the IBE must be introduced into the model by direct inclusion of variable atmospheric pressure into the equations of motion.

[39] Figure 15 shows results of 2-D SL simulations at 30 stations with and without IBE for 1960–present. Differences between these two model runs reflect "errors" associated with neglecting the IBE in the 2-D model simulation. The correlation of SL time series between the two model runs at 30 coastal stations is shown in the middle panel. Correlation is small in the Kara Sea, which is significantly deeper than other Siberian Seas and where SSH reaction to the IBE is stronger than SSH change due to wind forcing. In the Laptev and East Siberian Seas, the role of wind forcing dominates over the role of the IBE, and the total SL variability is due to wind effects. This explains the high correlations between simulated SSH time series without and with IBE.

[40] There is an interesting question about possible sea ice dynamics forced by changes in atmospheric pressure. *Leppäranta* [2005] has analyzed typical scales (see Table 5.5 in his book) of different forces influencing sea ice drift and pointed out that the air pressure term influencing sea ice motion is minor and is not commonly listed in the equations of sea ice motion. On the other hand, in the majority of 3-D coupled ice-ocean models the atmospheric pressure term is also neglected. The inclusion of the IBE in the governing equations of the water dynamics has to be accompanied by corresponding inclusion of the IBE in the equations of sea ice dynamics [*Leppäranta*, 2005]. We have tested the role of the IBE factor in sea ice dynamics based on numerical experiments with our 2-D model. In these experiments, sea ice and water dynamics were simulated with atmospheric loading in both sea ice and ocean models versus the case when IBE was included only in the equations of water motion. In both cases, the system was forced by the atmospheric pressure term and wind forcing was neglected to obtain results not masked by wind forcing and nonlinear effects associated with sea ice redistribution and water motion.

[41] Figure 16 shows that changes in SSH associated with atmospheric pressure redistribution can affect sea ice drift if IBE is not included in the sea ice dynamics equations. Because of the influence of SL gradients (tilt in the sea surface) induced by atmospheric loading, sea ice drifts if atmospheric loading is neglected in sea ice dynamics. This figure illustrates this effect, showing monthly SSH and sea ice drift calculated under atmospheric loading forcing in 1961. One sees that artificial sea ice drift reaches up to 2 cm/s and acts to slow the wind-driven ice circulation.

[42] It is important to note that ocean reaction to atmospheric loading could be detected only at short timescales because at longer timescales atmospheric loading is balanced by SSH gradients and the ocean does not move under steady state atmospheric loading. But at daily and shorter timescales during periods of ocean adjustment to atmospheric loading, the ocean currents exist. Figure 17 shows some results of investigation of ocean dynamics associated with only IBE forcing in Bering and Fram Straits. Daily water transports can reach 9 Sv in Fram Strait and 0.2 Sv in Bering Strait. Unfortunately, we could not validate these estimates based on observations in Fram Strait because daily data are not presently available for water transports (U. Schauer, personal communication), but daily velocity change in Bering Strait is ±50 cm/s [*Woodgate et al.*, 2005] which is (assuming that strait width is ∼70 km and mean depth is ∼50 m) ±1.75 Sv. *Woodgate et al.* [2005] conclude that this variability is associated with wind forcing. The IBE related transport of 0.2 Sv is a part of this daily variability.

[43] Mean transports due to atmospheric loading for 1960–2000 are very small: 0.08 Sv with STD of 1.9 Sv in Fram Strait and −0.02 Sv with STD of 0.04 Sv in Bering Strait. Unfortunately, it is impossible to extract only the inverted barometer generated signal from the observational data to validate these results. Interestingly, these fluxes reflect the fact that SL in the Arctic Ocean increases due to long-term decrease of SLP over the ocean.

[44] Existing Arctic ocean and sea ice models do not take the inverted barometer effect into account. This factor together with tides plays an important role in the water dynamics of shallow Arctic areas in winter (about 8–9 months) because fast ice blocks direct wind influence on the water surface and only motions generated by varying atmospheric pressure and tidal forcing are possible.

[45] In the deep ocean, the IBE due to moving cyclones and generation of long waves in the ocean is even more pronounced at the synoptic timescale. We also speculate that the atmospheric loading effect at relatively short timescales corresponding to the adjustment of SSH to atmospheric

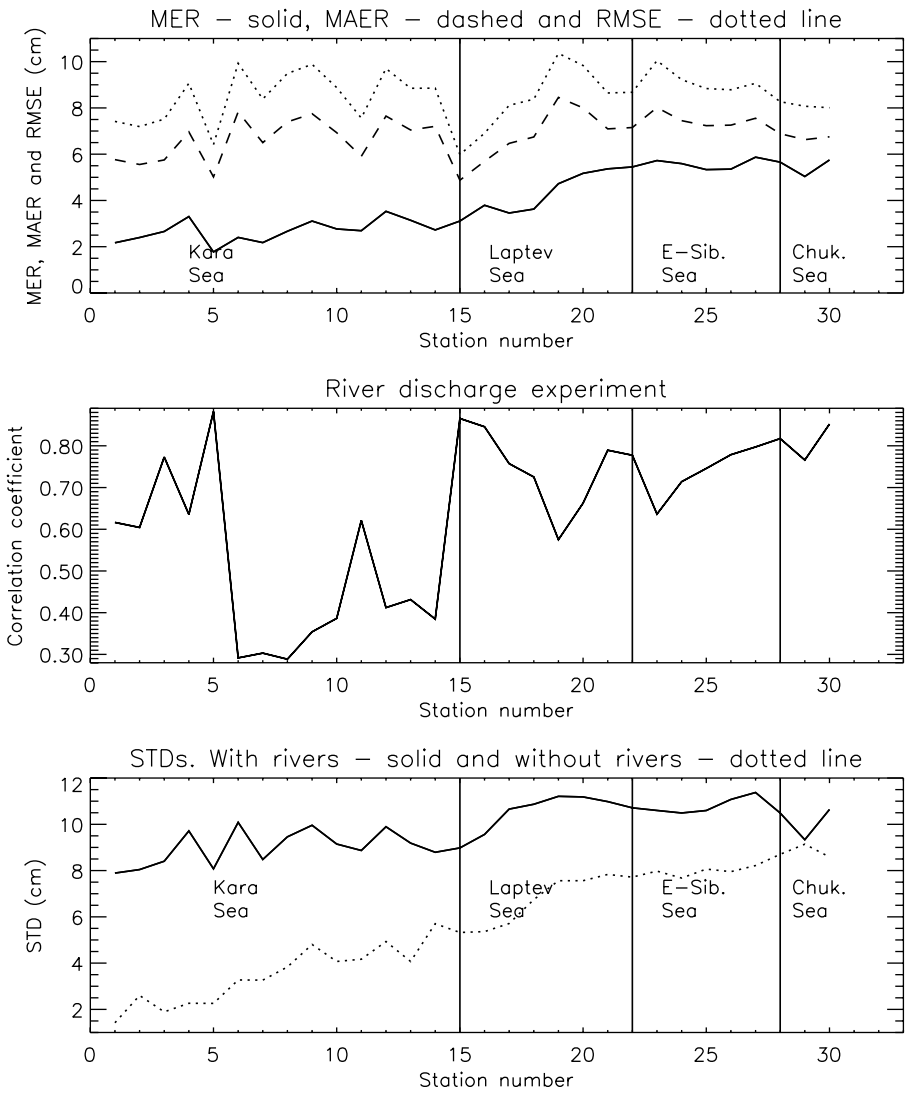

Figure 12. Statistical parameters characterizing results of the "river discharge" experiment. Upper panel shows mean error (MER), mean absolute error (MAER), and root mean square error (RMSE) due to simulations of SL variability without river runoff in the 2-D model. All other model parameters were left unchanged. Middle panel shows correlation coefficients between the control 2-D model run and a model run without river discharge. Bottom panel shows SSH standard deviations (cm) for the control and experimental model run without river discharge.

loading and generating water motions at all depths similar to tides can play an important role in ocean mixing (see *Holloway and Proshutinsky* [2007] where tidal effects were estimated). For example, Fram Strait water transport due to M_2 tidal forcing is approximately 5.6 Sv and is comparable with the transport driven by atmospheric pressure changes shown above.

5.4. Bering Strait Inflow and the Circulation of the Beaufort Gyre

[46] The Bering Strait inflow plays an important role not only in the dynamics of the Chukchi Sea (by providing a "through flow" circulation in this region, a heat flux that influences ice conditions, and a freshwater flux that adds more fresh water to the Beaufort Gyre); it also influences the dynamics of the entire Arctic Ocean by being driven by a pressure gradient associated with the SL difference between the Pacific and Atlantic Oceans [*Coachman et al.*, 1975; *Proshutinsky*, 1986]. It is interesting that the water circulation driven by this barotropic pressure gradient influences the Beaufort Sea circulation by acting against anticyclonic winds in winter, and in unison in summer to rotate the entire Beaufort Gyre and drive it cyclonically. A simple experiment with the 2-D barotropic model, described below, confirms these conclusions.

[47] Figure 18 shows SSH and water motion in the Arctic Ocean under the influence of a SL gradient of approximately 1 m between the Pacific and Atlantic Oceans. In order to provide this water transport in Bering Strait, 1 m of SSH is prescribed along the model's open boundary in the Bering Sea. Along the open boundary in the North Atlantic Ocean a radiation condition is prescribed; i.e. outflow or inflow dynamically compensates any water mass loss or gain along

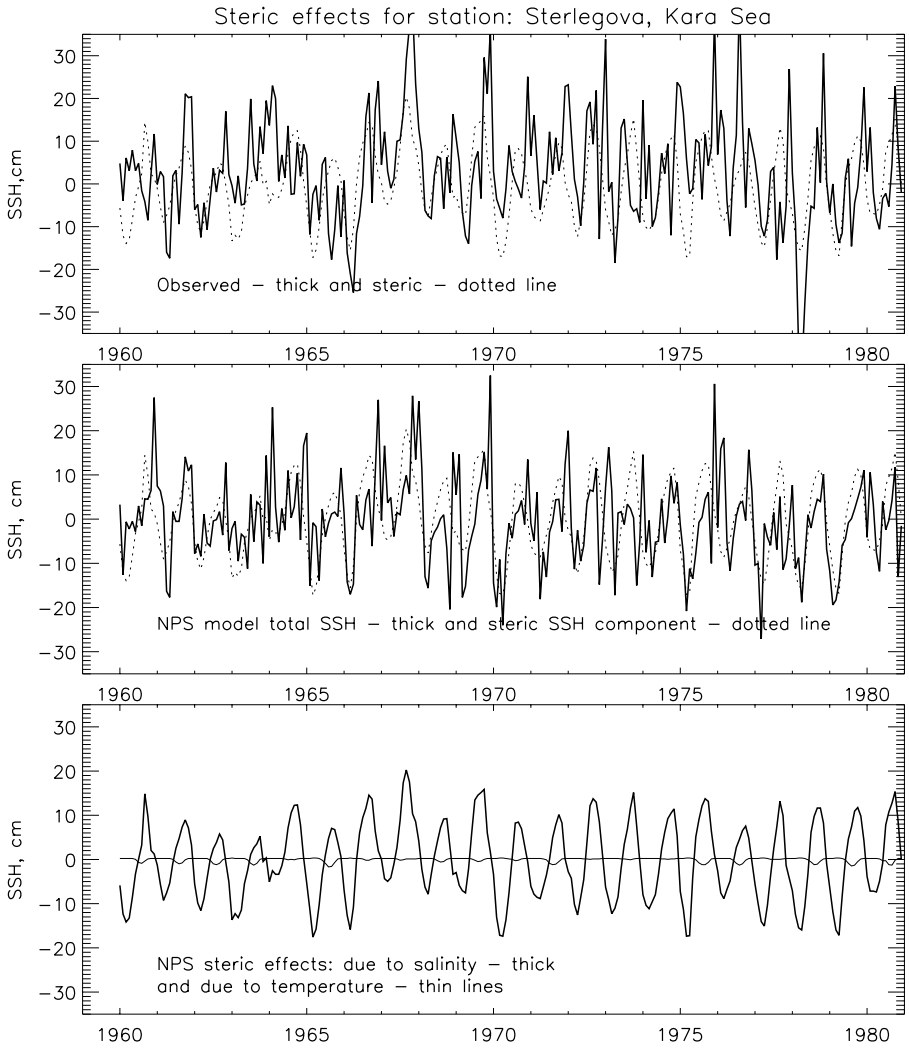

Figure 13a. Results of SL simulations for station Sterlegova, Kara Sea. Upper panel shows monthly SSH variations due to steric effects from the NPS model as a dotted line. Thick line shows SSH from observations without corrections. Middle panel shows the total SSH from the NPS model (solid line) and the steric component from the NPS model (dotted line). Bottom panel shows NPS model steric effect due to salinity change (thick line) and due to temperature change (thin line).

this boundary. This experiment shows that the strong inflow of water via Bering Strait results in the formation of a coastal circulation along the shelves and continental margins of the Chukchi and Beaufort Seas. In summer, this circulation coincides with the cyclonic winds and intensifies. In winter, this flow can be blocked by winds completely but, in general, it slows the Beaufort Gyre's anticyclonic ice and water circulations. Figure 18 also shows strong SL gradients over the Chukchi and Beaufort Sea shelf regions. Variability of the Bering Strait transport influenced by, for example, atmospheric processes in the Bering Sea will result in SL changes along Alaskan coastline and in the Chukchi and Beaufort Seas. It would be difficult to explain these changes if the Bering Strait inflow is not considered in the model or if it does not change seasonally and at longer timescales.

[48] The pressure gradient associated with the Bering Strait inflow should drive the entire circulation of the Beaufort Gyre from the surface to bottom layers cyclonically and can be responsible for one of the mechanisms influencing redistribution of the Pacific waters in the Canada Basin. Assuming that the surface layer of the Arctic Ocean in the Canada basin is driven by winds anticyclonically and that the depth of the Ekman layer is approximately 25–30 m, it can be concluded that below 40–50 m, the Pacific water circulates cyclonically and its circulation speed depends on the variability of the Bering Strait inflow. This inflow is also regulated by the wind regime over the Chukchi Sea and good correlation between wind forcing and circulation of Pacific waters is expected. It is also expected that in summer with diminishing anticyclonic winds, the cyclonic circulation of Pacific waters and all waters below the Ekman layer (including Atlantic and deep waters) intensifies.

5.5. Fast Ice

[49] Fast ice is an important component of the Arctic sea ice. Assuming that a fast ice region usually extends to approximately 25 m of water depth (*Wadhams* [2002]

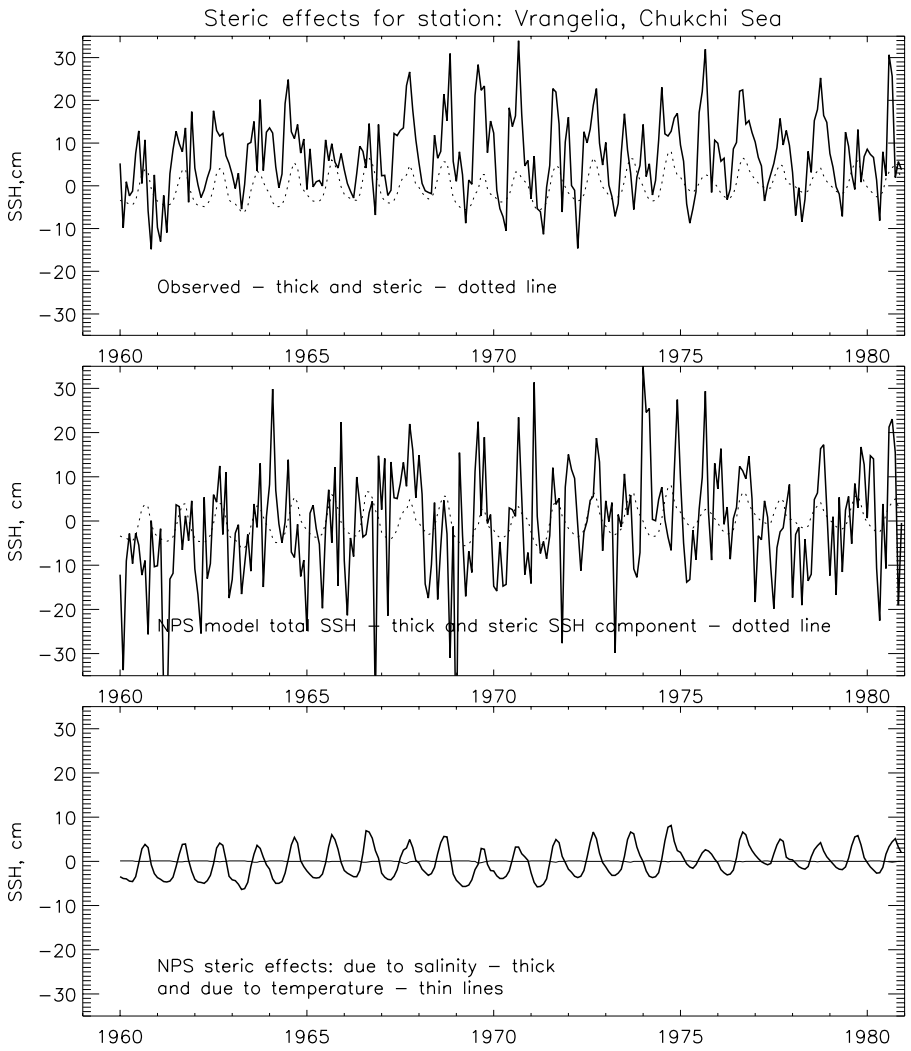

Figure 13b. Results of SL simulations for station Vrangelia, Chukchi Sea. Upper panel shows monthly SSH variations due to steric effects from the NPS model as a thin line. Thick line shows SSH from observations without corrections. Middle panel shows the total SSH from the NPS model (solid line) and the steric component from the NPS model (dotted line). Bottom panel shows NPS model steric effect due to salinity change (thick line) and due to temperature change (thin line).

determines this as 18–27 m and *Konig et al.* [2007] estimate this as depth more than 30 m; *Mahoney et al.* [2007] for 1996–present found that this depth is 18 m along Beaufort Sea coastline), we calculated areas of possible fast ice occupation using the topographical data obtained from the International Bathymetric Chart of the Arctic Ocean (IBCAO) at http://www.ngdc.noaa.gov/mgg/bathymetry/arctic/. The IBCAO data is provided at minute intervals between 64°N and 90°N and all longitudes. Calculations showed that the ocean area with the depth less than 25 m occupies 11% of the Arctic Ocean and 29% of the Arctic shelves (depth less than 200m). This is in agreement with estimations of Y. Yu and H. L. Stern from University of Washington (http://arcticchamp.sr.unh.edu/featuredproject/archive/yu_stern.s html) who showed that the fast ice area in the Northern Hemisphere is approximately 1,800,000 km^2. Assuming that the total winter area of the Arctic sea ice is approximately 14,000,000 km^2, the fast ice area is approximately 13% of the Northern Hemisphere area of sea ice coverage.

[50] In the Russian Arctic marginal seas (Kara, Laptev, East Siberian and Chukchi), fast ice occupies up to 40% of their regions. Fast ice protects the sea surface from wind stress, and damps tidal motion and winter storm surges. Fast ice influences the distribution of river runoff by channeling and damming the buoyant flow. Strong upwelling and downwelling events observed at the boundary of fast ice increase mixing and heat fluxes from the ocean deep layers. Existing models tend to have higher momentum flux to the ocean than in the real world because their "fast ice" drifts instead of remaining fast. Time series of fast-ice extent, thickness and date of formation or decay can thus be of considerable value as integral measures of climate variability and change. This has long been recognized and has motivated longer-term programs devoted to the acquisition of fast-ice data at selected locations in the North American and Siberian Arctic [*Zubov*, 1945; *Bilello*, 1980; *Brown and Cote*, 1992;

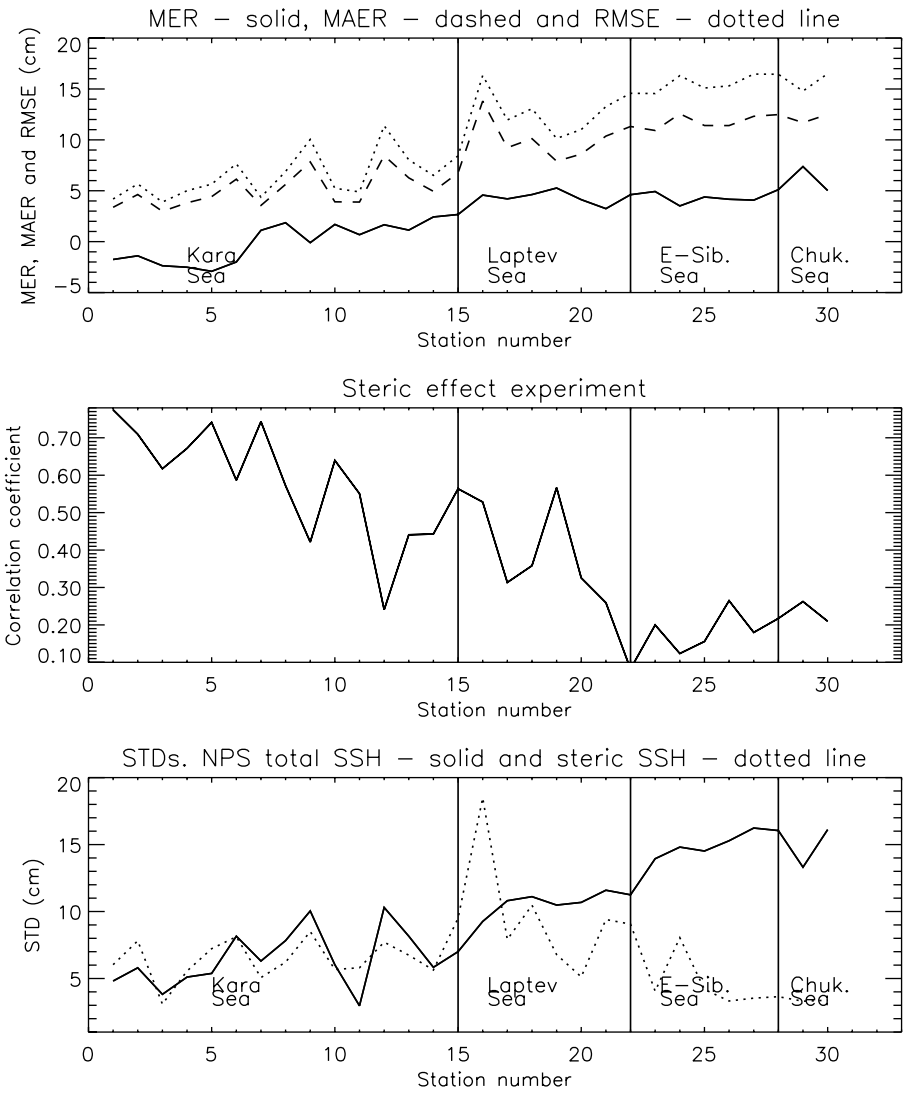

Figure 14. Statistical parameters characterizing the role of steric effects in SL variability from the NPS model. Upper panel shows mean error (MER), mean absolute error (MAER), and root mean square error (RMSE) as a result of comparing observational data with SSH due to steric effects from the NPS model. Middle panel shows correlation coefficients between observed SSH and steric SSH from the NPS model. Bottom panel shows SSH standard deviations (cm) for the analyzed data sets.

Flato and Brown, 1996; *Konig et al.*, 2007]. Because of its location at a critical juncture between land and ocean, the importance of the Arctic fast-ice cover extends to a number of other coastal processes that figure prominently in the context of climate variability and change. Thus, the location of the fast ice edge delineates the boundary of a system of coastal polynyas prominent both in the Laptev Sea and parts of the Alaskan Arctic [*Zakharov*, 1966; *Barry et al.*, 1979; *Reimnitz et al.*, 1994]. The Great Siberian Polynya in the Laptev and East Siberian Seas could be a product of the interaction between fast ice and winds. During winter, surface winds create upwelling along the fast ice edge and Atlantic Waters penetrate to the shelf, creating the Great Siberian Polynya which releases heat [*Proshutinsky*, 1993; *Kowalik and Proshutinsky*, 1994]. The salt flux originating from these localized areas of high ice production affects the thermohaline circulation on the shelf and is a major factor in the ventilation of intermediate and deep water layers in the Arctic Basin [*Cavalieri and Martin*, 1994; *Schauer et al.*, 1997; *Dethleff et al.*, 1998]. Shifting the location of these polynyas through changes in the fast-ice regime can thus have important implications for production and pathways of dense water masses. In the existing models without fast ice, all of these processes are shifted toward the coast and apparently do not influence oceanic circulation and water mass formation.

[51] Figure 19 shows monthly statistical parameters characterizing differences between SL time series calculated with and without fast ice in the 2-D model. It confirms the mechanical role of fast ice in the SL changes discussed above. This figure shows that island stations where the fast ice is usually absent do not show any substantial changes in SL behavior relative to the control model run. But coastal stations are influenced significantly (errors between experi-

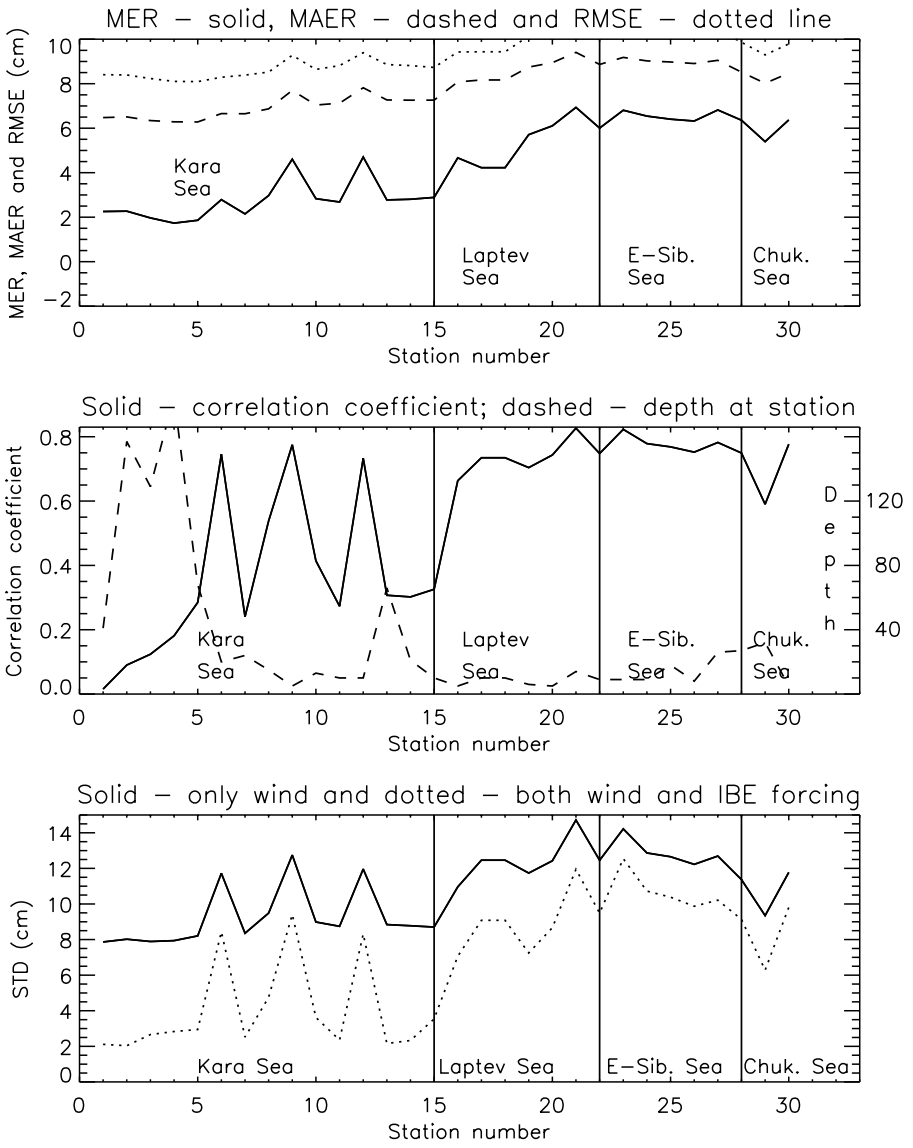

Figure 15. Statistical parameters characterizing results of the "inverted barometer effect" experiment. Upper panel shows mean error (ME), mean absolute error (MAE), and root mean square error (RMSE) associated with neglecting the IBE effect. Middle panel shows correlation coefficients between the control 2-D model run with IBE and a model run without IBE. Bottom panel shows SSH standard deviations (cm) for the control and the run without IBE.

ments reach maximum, correlation coefficients decrease and sea level STDs of the stations influenced by fast ice are suppressed) in seas with fast ice, particularly in the Laptev and East Siberian Seas where fast ice extent reaches for hundreds of kilometers.

6. Conclusions and Recommendations

[52] In general, AOMIP ocean models with a free surface are able to simulate variability of SSH reasonably well but several improvements are needed to decrease model errors. Here we do not discuss any issues associated with model forcing fields and parameters, accuracy of numerical approximations, or parameterizations of internal ice and ocean processes. Some of these are discussed in other publications presented in this AOMIP special section. We focus on recommendations relatively inexpensive to implement (without significant changes in model codes) and possibly useful at least from the perspective of more complete model physics.

[53] 1. The first issue is model resolution, specifically the resolution of ocean bathymetry. It is found that in order to reproduce variability of SSH at the locations of tide gauges in the shallow Arctic seas, it is important to have a minimum depth of no more than 10 m. This change would allow models to more correctly reproduce SL variability associated with wind forcing and atmospheric loading (extreme magnitudes and phases of long waves or storm surges), propagation of waves resulting from river runoff (especially in June–July when river discharges reach their maximum and SL rises dramatically in river deltas), and formation of anomalies in water temperature and salinity

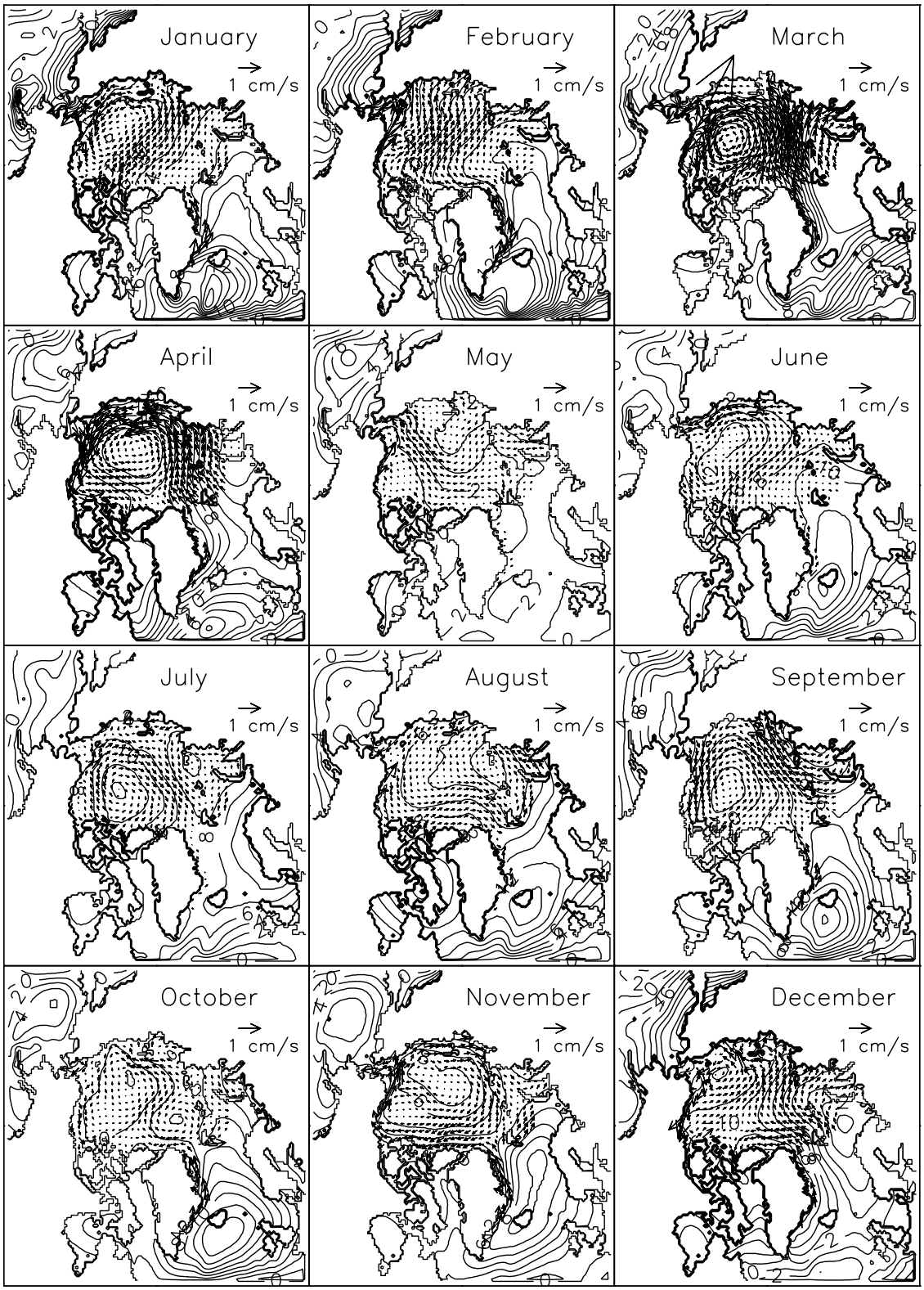

Figure 16. Numerical model results illustrating errors in sea ice drift if atmospheric loading (IBE) is taken into account in water motion equations but neglected in sea ice dynamics. The model generates artificial ice motion along isobars against geostrophic wind.

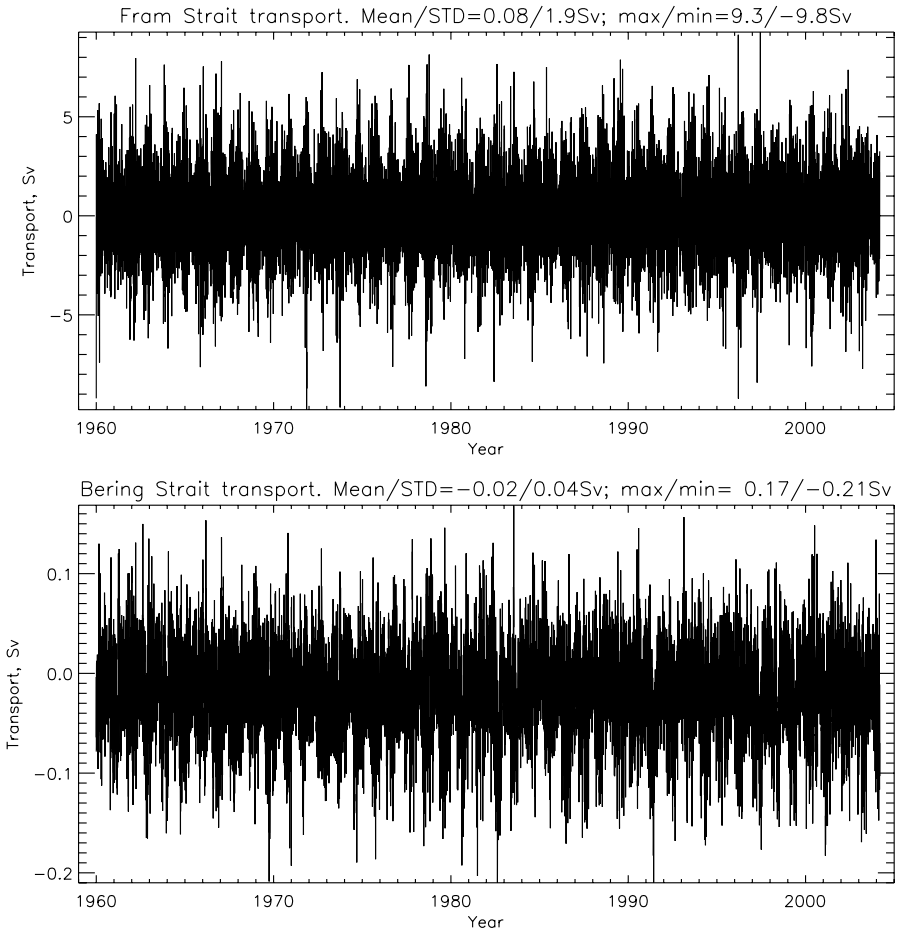

Figure 17. (top) Fram and (bottom) Bering Strait daily water transports (Sv) forced by atmospheric loading only.

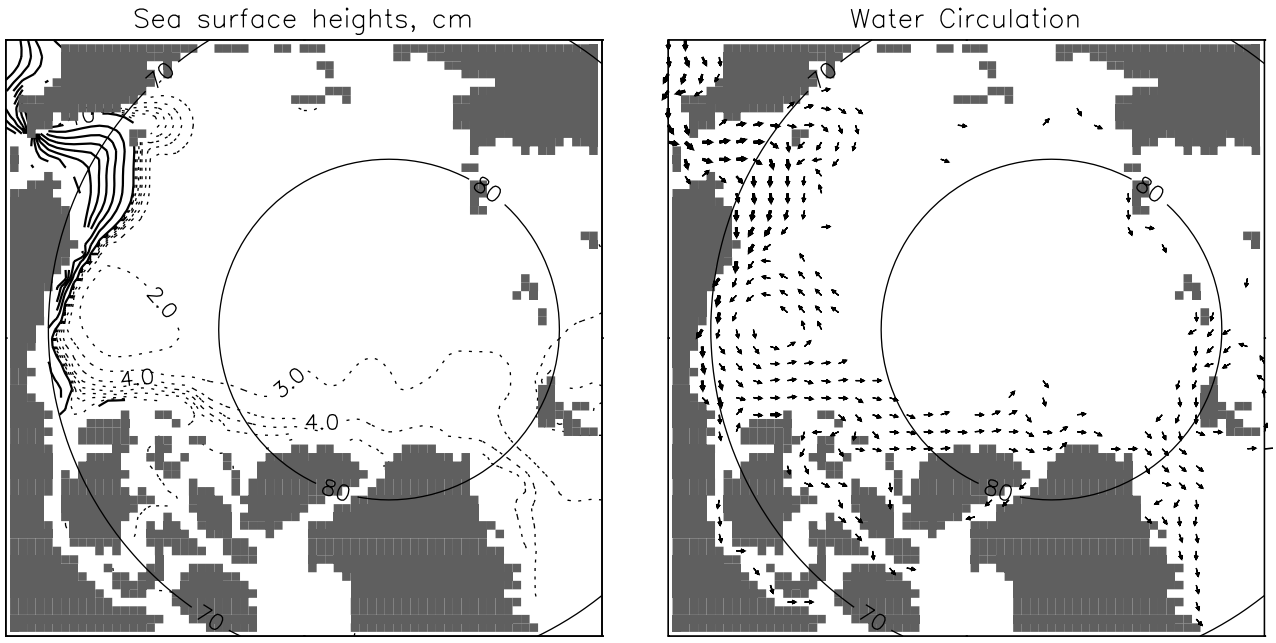

Figure 18. Sea surface (left) heights and (right) currents due to Bering Strait inflow. Solid contour interval is 10 cm, and dotted contours indicate SSH less than 10 cm with an interval of 1 cm. Vectors with velocities less then 0.25 cm/s are not shown. Vectors with velocities between 1 cm/s and 0.25 cm/s are shown in thin lines, and then vector thickness increases proportionally with the velocity multiplied by 5.

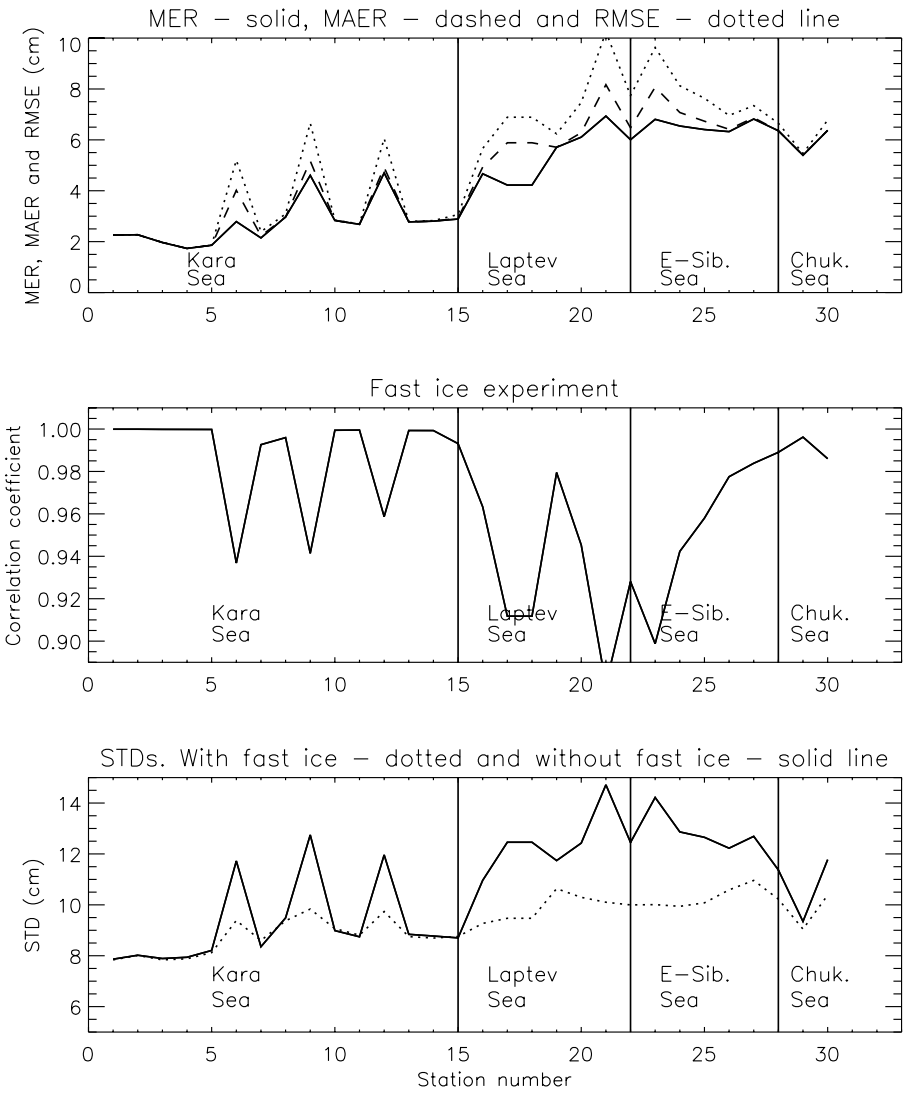

Figure 19. Statistical parameters characterizing results of the "fast ice" experiment. Upper panel shows mean error (ME), mean absolute error (MAE), and root mean square error (RMSE) associated with neglecting the fast ice effect. Middle panel shows correlation coefficients between the control 2-D model run with fast ice and a model run without fast ice. Bottom panel shows SSH standard deviations (cm) for the control and the run without fast ice.

fields, coastal circulations and sea ice regimes. Increasing the models' vertical resolution, recommended for instance by *Zhang and Steele* [2007], would improve simulations of Arctic halocline and processes of heat exchange between Arctic waters and the atmosphere and between surface Arctic waters and deeper layers.

[54] 2. We also recommend that models take into account forcing associated with atmospheric loading (IBE). This effect is responsible for SL variability not only at synoptic timescales (for example, storms) but also changes in SL at seasonal, interannual and long-term timescales. This is especially important for the Arctic Ocean which is separated from the rest of the World Ocean by relatively narrow or shallow straits that modify long wave propagation to the Arctic Ocean from the North Atlantic and Pacific Oceans. Studies by *Yoshida and Hirose* [2006] demonstrate that inclusion of the Arctic Ocean in a global ocean barotropic model affects the northwestern Atlantic Ocean through the propagation of Kelvin waves. Air pressure induces sea surface variability stronger than that forced by surface wind for most of the global oceans except the Southern Ocean. In the Arctic Ocean, the pressure induced component is responsible for more than 90% of the variability forced both by pressure and wind according to this publication. The water mass oscillates through the strait between the Arctic Ocean and the North Atlantic Ocean with a period of 10 days and an amplitude of about 8.5 Sv. Average SL lags because the basin- wide isostatic adjustment is only established by limited water exchange through the strait. Our 2-D regional model results confirm these conclusions (Figure 17).

[55] Inclusion of atmospheric loading in the oceanic model module must be accompanied by an atmospheric loading effect in the sea ice dynamics model module, to avoid artificial sea ice motion.

[56] Short period variability of ocean dynamics due to the IBE could be comparable with the effects of tidal forcing discussed by *Proshutinsky* [1993], *Kowalik and Proshutinsky* [1994], *Heil and Hibler* [2002], and *Holloway and Proshutinsky* [2007].

[57] 3. Our experiments with the 2-D barotropic model investigated the dynamical effects of fast ice. In these experiments, the fast-ice extent influences SL dynamics mechanically, primarily by damping the magnitude of long waves propagating under fast ice (storm surges, tides). These effects are important for the shallow Siberian seas and we recommend inclusion of fast ice in 3-D model simulations. The potential for upwelling and downwelling at ice boundaries was noted by *Gammelsrod et al.* [1975] using a homogeneous ocean model with stationary ice. *Clarke* [1978] and *Niebauer* [1982] extended these results to include stratification and meltwater, respectively. *Carmack and Chapman* [2003] concluded that the efficiency of shelf/basin exchange is strongly moderated by the location of the ice edge relative to underlying topography. Baroclinic effects are also important along the fast ice edge and we recommend investigating them with several AOMIP models. The implementation or parameterization of fast ice in 3-D models is an interesting and difficult task but it could be solved step by step, first implementing the relatively primitive empirical approach employed in our 2-D model simulations, then developing a model of fast ice formation and decay.

[58] 4. Bering Strait inflow and river runoff are important for the dynamics and thermodynamics of both sea ice and the ocean via their influence on freshwater and heat balances. We speculate and demonstrate that the pressure gradient associated with the Bering Strait inflow should drive the entire circulation of the Beaufort Gyre from the surface to bottom layers cyclonically with a speed of 1–2 cm/s and can be responsible for one of the mechanisms influencing redistribution of the Pacific waters in the Canada Basin. Almost all AOMIP models (except the NPS model version and the Alfred Wegener Institute model not discussed here) include Bering Strait and riverine influences, but this subject has not been investigated thoroughly in the scientific literature and more studies are needed.

[59] 5. Observations from 9 tide gauge stations representing SL conditions in the Siberian seas (Kara, Laptev, and East Siberian) show that SL is rising in this region at a rate of 0.25 cm/yr for the 1954–2006 period. There is also a well pronounced decadal variability in the observed SL time series that correlates with the AO [*Proshutinsky et al.*, 2004]. In agreement with AO behavior, the SL dropped significantly after 1990 but started rising again in 2002. This fact was confirmed by *Scharroo et al.* [2006] based on satellite observations over the entire Arctic Ocean. The SL time series obtained from this study revealed a negative SSH trend of −0.217 cm/yr (region from 60°N to 82°N) for the period 1995 to 2003. This is consistent with Figure 1. In contrast, the coastal data shows that from 2000 to 2006 the SL rise rate has increased despite a steady, low AO index. Because of the large interannual variability, it is difficult to evaluate the significance of this change. We anticipated that AOMIP model results would allow us to explain the recently observed SL variability, but significant differences among model results enable us only to speculate that the central Arctic SL drop registered by satellites could be associated with steric effects.

[60] **Acknowledgments.** We thank Greg Holloway and Ruediger Gerdes for their review of this paper. The manuscript has been significantly improved as a result of their critical comments and helpful recommendations. This research is supported by the National Science Foundation Office of Polar Programs (under cooperative agreements OPP- 0002239 and OPP-0327664) with the International Arctic Research Center, University of Alaska Fairbanks, and by the Climate Change Prediction Program of the Department of Energy's Office of Biological and Environmental Research. The development of the UW model is also supported by NASA grants NNG04GB03G and NNG04GH52G and NSF grants OPP-0240916 and OPP-0229429.

References

Barry, R. G., R. E. Moritz, and J. C. Rogers (1979), The fast ice regimes of the Beaufort and Chukchi Sea coasts, Alaska, *Cold Reg. Sci. Technol.*, *1*, 129–152.

Bilello, M. A. (1980), Maximum thickness and subsequent decay of lake, river and fast ice in Canada and Alaska, *CRREL Rep.*, *80-6*, 1–160.

Blumberg, A. F., and G. L. Mellor (1987), A description of a three- dimensional coastal ocean circulation model, in *Three-Dimensional Coastal Ocean Models*, *Coastal Estuarine Stud.*, vol. 4, edited by N. S. Heaps, 208 pp., AGU, Washington, D. C.

Brown, R. D., and P. Cote (1992), Interannual variability of landfast ice thickness in the Canadian High Arctic, 1950–89, *Arctic*, *45*, 273–284.

Carmack, E., and D. C. Chapman (2003), Wind-driven shelf/basin exchange on an Arctic shelf: The joint roles of ice cover extent and shelf-break bathymetry, *Geophys. Res. Lett.*, *30*(14), 1778, doi:10.1029/2003GL017526.

Carrere, L., and F. Lyard (2003), Modeling the barotropic response of the global ocean to atmospheric wind and pressure forcing: Comparisons with observations, *Geophys. Res. Lett.*, *30*(6), 1275, doi:10.1029/2002GL016473.

Cavalieri, D. J., and S. Martin (1994), Contribution of Alaskan, Siberian, and Canadian coastal polynyas to the cold halocline layer of the Arctic Ocean, *J. Geophys. Res.*, *99*, 18,343–18,362.

Clarke, A. J. (1978), On wind-driven quasi-geostrophic water movement at fast ice edges, *Deep Sea Res.*, *25*, 41–51.

Coachman, L. K., K. Aagaard, and R. B. Tripp (1975), *Bering Strait: The Regional Physical Oceanography*, 172 pp., Univ. of Wash. Press, Seattle.

Dethleff, D., P. Loewe, and E. Kleine (1998), The Laptev Sea flaw lead - Detailed investigation on ice formation and export during 1991/92 winter season, *Cold Reg. Sci. Technol.*, *27*, 225–243.

Dvorkin, E. N., Y. V. Zakharov, and N. V. Mustafin (1978), On the causes of seasonal and multiyear variability of sea level in the Laptev and East Siberian Seas (in Russian), *Trudy AARI*, *349*, 60–68.

Dvorkin, E. N., Y. V. Zaharov, and N. V. Mustafin (1983), Seasonal and long-term variability of SL in the Arctic seas, *Problems Arct. Antarct.*, *60*, 10–16.

Dvorkin, E. N., S. Y. Kachanov, and N. P. Smirnov (2000), North Atlantic Oscillation and long-term variability of SL in the Arctic seas, *Sov. Meteorol. Hydrol.*, *3*, 78–84.

Flato, G. M., and R. D. Brown (1996), Variability and climate sensitivity of landfast Arctic sea ice, *J. Geophys. Res.*, *101*, 25,767–25,777.

Gammelsrod, T., M. Mork, and L. P. Roed (1975), Upwelling possibilities at an ice edge: Homogenous model, *Mar. Sci. Commun.*, *1*, 115–145.

Golubeva, E., and G. Platov (2007), On improving the simulation of Atlantic Water circulation in the Arctic Ocean, *J. Geophys. Res.*, *112*, C04S05, doi:10.1029/2006JC003734.

Häkkinen, S., and C. A. Geiger (2000), Simulated low-frequency modes of circulation in the Arctic Ocean, *J. Geophys. Res.*, *105*, 6549–6564.

Häkkinen, S., and G. L. Mellor (1992), Modeling the seasonal variability of the coupled Arctic ice–ocean system, *J. Geophys. Res.*, *97*, 20,285–20,304.

Heil, P., and W. D. Hibler (2002), Modeling the high-frequency component of Arctic sea-ice drift and deformation, *J. Phys. Oceanogr.*, *32*(11), 3039–3057.

Hibler, W. D., III (1979), A dynamic thermodynamic sea ice model, *J. Phys. Oceanogr.*, *9*, 815–846.

Holloway, G., and A. Proshutinsky (2007), Role of tides in Arctic ocean/ice climate, *J. Geophys. Res.*, *112*, C04S06, doi:10.1029/2006JC003643.

Holloway, G., et al. (2007), Water properties and circulation in Arctic Ocean models, *J. Geophys. Res.*, *112*, C04S03, doi:10.1029/2006JC003642.

Hunke, E. C., and M. Holland (2007), Global atmospheric forcing data for Arctic ice-ocean modeling, *J. Geophys. Res.*, *112*, C04S14, doi:10.1029/2006JC003640.

Hunke, E. C., and W. H. Lipscomb (2004), CICE: the Los Alamos Sea Ice Model, Documentation and Software User's Manual, v.3.1, *Tech. Rep. LA-CC- 98-16*, T-3 Fluid Dyn. Group, Los Alamos Natl. Lab., Los Alamos, N. M.

Intergovernmental Panel on Climate Change (IPCC) (2001), *Climate Change 2001: The Scientific Basis - Contribution of Working Group I to the Third Assessment Report of IPCC*, 994 pp., Cambridge Univ. Press, New York.

Jackett, D. R., and T. J. McDougall (1995), Minimal adjustment of hydrographic profiles to achieve static stability, *J. Atmos. Oceanic Technol.*, *12*(4), 381–389.

Karcher, M., F. Kauker, R. Gerdes, E. Hunke, and J. Zhung (2007), On the dynamics of Atlantic Water circulation in the Arctic Ocean, *J. Geophys. Res.*, doi:10.1029/2006JC003630, in press.

Konig, B. C., A. Ahmed, and D. M. Holland (2007), A climatology and analysis of Arctic landfast sea-ice data, *Atmos. Ocean*, in press.

Kowalik, Z., and A. Y. Proshutinsky (1994), The Arctic Ocean tides, in *The Polar Oceans and Their Role in Shaping the Global Environment*, *Geophys. Monogr. Ser.*, vol. 85, edited by O. M. Johannessen, R. D. Muench, and J. E. Overland, pp. 137–158, AGU, Washington, D. C.

Large, W. G., J. C. McWilliams, and S. C. Doney (1994), Oceanic vertical mixing: A review and a model with a nonlocal boundary layer parameterization, *Rev. Geophys.*, *32*, 363–403.

Leppäranta, M. (2005), *The Drift of Sea Ice*, Springer, New York.

Mahoney, A., H. Eicken, A. G. Gaylord, and L. Shapiro (2007), Alaska landfast sea ice: Links with bathymetry and atmospheric circulation, *J. Geophys. Res.*, *112*, C02001, doi:10.1029/2006JC003559.

Manual for Stations and Gauges of the Hydrometeorological Service, (1968) *Hydrometeoizdat*, *9*(1), 242 pp.

Maslowski, W., B. Newton, P. Schlosser, A. J. Semtner, and D. G. Martinson (2000), Modeling recent climate variability in the Arctic Ocean, *Geophys. Res. Lett.*, *27*(22), 3743–3746.

Niebauer, H. J. (1982), Wind- and melt-driven circulation in a marginal sea ice edge frontal system: A numerical model, *Cont. Shelf Res.*, *1*, 49–98.

Pacanowski, R., and S. G. H. Philander (1981), Parameterization of vertical mixing in numerical models of tropical oceans, *J. Phys. Oceanogr.*, *11*(11), 1443–1451.

Parkinson, C. L., and W. M. Washington (1979), A large scale numerical model of sea ice, *J. Geophys. Res.*, *84*, 311–337.

Parsons, A. R. (1995), On the Barents Sea polar front in summer and interpretations of the associated regional oceanography using an Arctic Ocean general circulation model, Ph.D. thesis, Nav. Postgrad. Sch., Monterey, Calif.

Pattullo, J., W. Munk, R. Revelle, and E. Strong (1955), The seasonal oscillation in sea level, *J. Mar. Res.*, *14*, 88–156.

Pavlov, V. K., and P. V. Pavlov (1999), Features of seasonal and interannual variability of SL and water circulation in the Laptev Sea, in *Land–Ocean Systems in the Siberian Arctic: Dynamics and History*, edited by H. Kassens et al., pp. 3–16, Springer, New York.

Polyakov, I., A. Proshutinsky, and M. Johnson (1999), The seasonal cycles in two regimes of Arctic climate, *J. Geophys. Res.*, *104*(C11), 25,761–25,788.

Proshutinsky, A. Y. (1978), On the computation of storm surges in the shelf zone of the Arctic Seas, *Sov. Meteorol. Hydrol.*, *8*, 54–60.

Proshutinsky, A. Y. (1986), On the problem of calculating the storm surge fluctuations of SL and water circulation in the Chukchi Sea, *Sov. Meteorol. Hydrol.*, *1*, 54–61.

Proshutinsky, A. Y. (1993), *Arctic Ocean Sea Level Variability*, 216 pp., Gidrometeoizdat, St. Petersburg.

Proshutinsky, A. Y., and M. Johnson (1997), Two circulation regimes of the wind-driven Arctic Ocean, *J. Geophys. Res.*, *102*, 12,493–12,514.

Proshutinsky, A., V. Pavlov, and R. Bourke (2001), Sea level rise in the Arctic Ocean, *Geophys. Res. Lett.*, *28*(11), 2237–2240.

Proshutinsky, A., I. M. Ashik, E. N. Dvorkin, S. Häkkinen, R. A. Krishfield, and W. R. Peltier (2004), Secular sea level change in the Russian sector of the Arctic Ocean, *J. Geophys. Res.*, *109*, C03042, doi:10.1029/2003JC002007.

Rasmusson, E. M., and K. Mo (1996), Large scale atmospheric moisture cycling as evaluated from NMC global analysis and forecast products, *J. Clim.*, *9*, 3276–3297.

Reimnitz, E., D. Dethleff, and D. Nornberg (1994), Contrasts in Arctic shelf sea-ice regimes and some implications: Beaufort Sea and Laptev Sea, *Mar. Geol.*, *119*, 215–225.

Scharroo, R., A. L. Ridout, and S. W. Laxon (2006), Arctic sea level change from satellite altimetry, *Eos Trans. AGU*, *87*(36), Jt. Assem. Suppl., Abstract G21A-02.

Schauer, U., R. D. Muench, B. Rudels, and L. Timokhov (1997), Impact of eastern Arctic shelf waters on the Nansen Basin intermediate layers, *J. Geophys. Res.*, *102*, 3371–3382.

Smith, R. D., and P. R. Gent (Eds.) (2002), Reference manual for the Parallel Ocean Program (POP): Ocean component of the Community Climate System Model (CCSM2.0 and 3.0), Natl. Cent. for Atmos. Res., Boulder, Colo. (Available at http://www.ccsm.ucar.edu/models/ccsm2.0.1/pop/)

Smith, R. D., J. K. Dukowicz, and R. C. Malone (1992), Parallel ocean general circulation modeling, *Physica D*, *60*, 38–61.

Vinogradova, N. T., R. M. Ponte, and D. Stammer (2007), Relation between sea level and bottom pressure and the vertical dependence of oceanic variability, *Geophys. Res. Lett.*, *34*, L03608, doi:10.1029/2006GL028588.

Vorobyov, V. N., S. Y. Kochanov, and N. P. Smirnov (2000), Seasonal and multiyear sea-level fluctuations in the Arctic Ocean, 113 pp., Minist. of Educ. of Russ. Fed., Saint Petersburg.

Wadhams, P. (2002), *Ice in the Ocean*, 351 pp., Gordon and Breach, New York.

Walsh, J. E., W. L. Chapman, and T. L. Shy (1996), Recent decrease of sea level pressure in the central Arctic, *J. Clim.*, *9*, 480–486.

Woodgate, R. A., K. Aagaard, and T. J. Weingartner (2005), Monthly temperature, salinity, and transport variability of the Bering Strait through flow, *Geophys. Res. Lett.*, *32*, L04601, doi:10.1029/2004GL021880.

Woodworth, P. L., et al. (Eds.) (1992), *Sea Level Changes: Determination and Effects*, *Geophys. Monogr. Ser.*, vol. 69, AGU, Washington, D. C.

Wunsch, C., and D. Stammer (1997), Atmospheric loading and the oceanic inverted barometer effect, *Rev. Geophys.*, *35*(1), 79107.

Yoshida, S., and N. Hirose (2006), Non-equilibrium sea level response to surface pressure loading in the high-latitude oceans, *Eos Trans. AGU*, *87*(36), Ocean Sci. Meet. Suppl., Abstract OS25Q-01.

Zakharov, V. F. (1966), The role of flaw leads off the edge of fast ice in the hydrological and ice regime of the Laptev Sea, *Oceanology*, *6*, 815–821.

Zhang, J., and D. A. Rothrock (2003), Modeling global sea ice with a thickness and enthalpy distribution model in generalized curvilinear coordinates, *Mon. Weather Rev.*, *131*(5), 681–697.

Zhang, J., and M. Steele (2007), Effect of vertical mixing on the Atlantic Water Layer circulation in the Arctic Ocean, *J. Geophys. Res.*, *112*, C04S04, doi:10.1029/2006JC003732.

Zhang, Y., W. Maslowski, and A. J. Semtner (1999), Impacts of mesoscale ocean currents on sea ice in high resolution Arctic ice and ocean simulations, *J. Geophys. Res.*, *104*, 18,409–18,429.

Zubov, N. N. (1945), *Arctic Ice*, Izd. Glavsevmorputi, Moscow.

I. Ashik, Arctic and Antarctic Research Institute, 198095 St. Petersburg, Russia.

S. Häkkinen, Goddard Space Flight Center, Greenbelt, MD 20771, USA.

E. Hunke and M. Maltrud, Los Alamos National Laboratory, Los Alamos, NM 87545, USA.

R. Krishfield and A. Proshutinsky, Department of Physical Oceanography, Woods Hole Oceanographic Institution, MS# 29, 360 Woods Hole Road, Woods Hole, MA 02543, USA. (aproshutinsky@whoi.edu)

W. Maslowski, Department of Oceanography, Naval Postgraduate School, Monterey, CA 93943-5122, USA.

J. Zhang, Polar Science Center, University of Washington, Seattle, WA 98105, USA.